



# Bioinspired pH-sensitive riboflavin controlled-release alkaline hydrogels based on blue crab chitosan: Study of the effect of polymer characteristics

Marwa Hamdi, Rim Nasri, S.M. Li, Moncef Nasri

## ► To cite this version:

Marwa Hamdi, Rim Nasri, S.M. Li, Moncef Nasri. Bioinspired pH-sensitive riboflavin controlled-release alkaline hydrogels based on blue crab chitosan: Study of the effect of polymer characteristics. International Journal of Biological Macromolecules, 2020, 152, pp.1252-1264. 10.1016/j.ijbiomac.2019.10.222 . hal-03790215

**HAL Id: hal-03790215**

**<https://hal.umontpellier.fr/hal-03790215>**

Submitted on 5 Oct 2022

**HAL** is a multi-disciplinary open access archive for the deposit and dissemination of scientific research documents, whether they are published or not. The documents may come from teaching and research institutions in France or abroad, or from public or private research centers.

L'archive ouverte pluridisciplinaire **HAL**, est destinée au dépôt et à la diffusion de documents scientifiques de niveau recherche, publiés ou non, émanant des établissements d'enseignement et de recherche français ou étrangers, des laboratoires publics ou privés.

# Bioinspired pH-sensitive Riboflavin controlled-release alkaline hydrogels based on blue crab chitosan: Study of the effect of wall polymer characteristics.

Marwa Hamdi <sup>a\*</sup>, Rim Nasri <sup>a,b</sup>, Suming Li <sup>c</sup>, Moncef Nasri <sup>a</sup>

<sup>a</sup> Laboratory of Enzyme Engineering and Microbiology, University of Sfax, National Engineering School of Sfax, 3038 Sfax, Tunisia.

<sup>b</sup> Higher Institute of Biotechnology of Monastir, University of Monastir, Monastir, Tunisia.

<sup>c</sup> European Institute of Membranes, UMR CNRS 5635, University of Montpellier, Place Eugene Bataillon, 34095 Montpellier Cedex 5, France.

**\* Corresponding author:** Marwa Hamdi, Laboratory of Enzyme Engineering and Microbiology, University of Sfax, National Engineering School of Sfax, B.P. 1173, 3038 Sfax, Tunisia. **Tel:** 216 25740373 / 216 54186612; **E-mail:** [marwahamdi50@yahoo.fr](mailto:marwahamdi50@yahoo.fr).

## Abstract

Recently, the application of natural biocompatible polymeric hydrogels for the conception of drug delivery matrices has attracted widespread interest. Thus, in the present study, riboflavin pH-sensitive drug delivery hydrogels were developed based on blue crab chitosan (Cs), via direct dissolution in alkali/urea aqueous solution at low temperatures. First, the effect of Cs characteristics in terms of acetylation degree (AD) and molecular weight (Mw) on the structural, mechanical, thermal, swelling and *in vitro* biodegradation of Cs-based hydrogels were studied. Data from overall analysis revealed that Cs with low AD and high Mw exhibited improved mechanical properties, as evidenced by the compressive and rheological behaviors tests, thermal resistance, swelling behavior and *in vitro* degradation kinetics. However, hydrogels pore sizes were reduced with the AD decrease and Mw increase. Additionally, hydrogels in PBS (pH 5.5) underwent quicker degradation, compared to those immersed in PBS (pH 7.4). In the drug delivery model, the kinetics of Riboflavin release, through the Cs-based hydrogels were monitored. The Riboflavin release exhibited a typical triphasic deliverance pattern, with significantly higher released amounts in more acidic systems. Therefore, drug encapsulation within the conceived pH-sensitive Cs-based hydrogels could provide suitable and promoting microenvironment for drugs delivery.

**Keywords:** Hydrogels; Acetylation degree and Molecular weight; Drug controlled-release.

## 1. Introduction

Hydrogels are three-dimensional hydrophilic polymeric networks with the ability to absorb large amounts of water or biological fluids [1-2]. Because of their high-water content, porosity and soft consistency, they closely simulate natural living tissues, more than any other class of synthetic biomaterials and thus open up many possibilities for applications in biomedical fields [3-5]. Physical hydrogels are distinguished from chemical hydrogels. The network of physical hydrogels is maintained through weak bonds (hydrophobic, hydrogen, ionic) that are not permanent because they are disconnected continuously depending on the medium (pH, temperature, ionic strength). The chemical hydrogels, however, have a network which is maintained by covalent crosslinks providing them a permanent character [6-7].

The high porosity that characterizes hydrogels can easily be adjusted by controlling the density of the crosslinks in their matrix and their affinity to water. Moreover, their porous structure allows to controllably loaded and released drugs [8-9]. The benefits of hydrogels for drug delivery applications include the possibility of controlled and sustained release, which permits a high local concentration of an active pharmaceutical ingredient (drug) to be maintained over a long period of time. The drug can be loaded into a hydrogel, and then released by several mechanisms: controlled release, controlled swelling, chemically controlled release and environmental release [10].

The rate of release can be managed by modifying some factors such as polymer concentration, crosslinking density, and water content. Some «smart» hydrogels have the ability to respond to external stimuli such as pH, temperature, ionic strength, etc., making them excellent site-specific active ingredient in delivery matrices for diseases prevention and treatment [11-12].

Hydrogels are of great interest for other biomedical applications because of the ability to control their swelling, mechanical properties, chemical and physical structures, crosslinking

density and porosity. Therefore, hydrogels are frequently used in tissue engineering for cell encapsulation or drug delivery, but as well as wound dressings, bioadhesives and biosensors [13-14]. In fact, hydrogels can serve as templates for directing cell behavior and promoting cell organization. In addition, the biocompatibility of hydrogels has generated a lot of interest in hygiene products, implants and soft contact lenses [15-16].

Advantageously, chitosan can be used in the preparation of hydrogels which serve as a matrix for the incorporation of active agents [17-19]. As part of this research, chitosan obtained by partial deacetylation of chitin was chosen. Chitosan-based hydrogels have shown important advantages in terms of drug delivery, as they allow site-specific and / or time-controlled administration for small and large drugs [17,20]. They offer, furthermore, many benefits, such as improving biosecurity and drug efficacy. Chitosan hydrogels can provide targeted delivery and improved stability of therapeutic agents against physiological degradation [17].

To the best of our knowledge, there is a lack of information in literature regarding the effect of acetylation degree and molecular weight on chitosan-based hydrogels, although several reports describe their developpement and application in particularly the biomedical field. Therefore, the objective of this work was the conception of high strength hydrogels based on chitosans with different acetylation degrees and molecular weights, to assess the effects of these two structural parameters on the properties of the resulting hydrogels. Subsequently, the selected hydrogel was applied for controlled release of Riboflavin with very interesting biological potential, as drug model.

## **2. Materials and methods**

### **2.1. Materials**

Riboflavin was purchased from LOBA CHEMIE (India) and the other used chemical reagents from commercial sources were of analytical grade and employed without further purifications.



## 2.2. Chitosans preparation and purification

Chitosans (Cs) from blue crab *Portunus segnis* shells were prepared in our laboratory, as described in our previous study [21]. Briefly, Cs with different AD were obtained through chitin N-deacetylation with NaOH 12.5 M at a w/v ratio of 1/10 at 140 °C, for 2, 3 and 5 h and produced Cs were named Cs I, Cs II and Cs III. After filtration, Cs was washed to neutrality and then dried for 12 h at 50 °C. Based on the nuclear magnetic resonance (<sup>13</sup>C NMR) analysis, ADs of 17%, 13% and 8% were reached for Cs I, Cs II and Cs III, respectively. Further, Cs were characterized by size exclusion chromatography (SEC-HPLC) and average molecular weights (Mw) of 125 600, 118 900 and 115 000 g mol<sup>-1</sup> were obtained for CsI, CsII and CsIII, respectively.

To generate Cs with different Mw, Cs, at different ADs, were hydrolyzed with Cellulase (10 U/g chitosan) in 0.5 N acetate-bicarbonate buffer (pH 5.2) at 55 °C, for 1 and 3 h, as described by Chang *et al.* [22] with slide modifications. The Cs obtained are lyophilized and analyzed to study the evolution of their molecular mass. The respective Mw were reported in **Table S1**.

Subsequently, Cs were purified according to the method described by Qian and Glanville [23]. Thus, crude Cs (6 g) was dissolved in 600 ml of HCl 0.1 M under stirring overnight at a temperature of 40 °C. The acidic solution was vacuum filtered to remove insoluble particles. Cs was then precipitated with NaOH 0.5 M under continuous stirring until approximately pH 8.5. Thereafter, 6 ml of 10% (w/v) sodium dodecyl sulfate (SDS) was added to the suspension and the mixture was heated at 95 °C for 5 min. After cooling at room temperature, the pH was adjusted to 10.0 with 0.5 M NaOH. The mixture was vacuum filtered and the hydrated Cs was washed 5 times with 600 ml of deionized water at 40 °C. A solution of barium chloride was used to confirm the absence of residual SDS in the filtrate. Finally, the obtained purified Cs were lyophilized, milled to powder and then sieved.

### 2.3. Conception of blue crab chitosan-based hydrogels

Hydrogels were prepared based on the freezing/thawing approach described by Duan *et al.* [5]. Briefly, Cs, derived from the action of Cellulase, were dissolved in an alkaline solution, widely used for the dissolution of cellulose and chitin, consisting of 4.5 wt. % LiOH, 7.5 wt. % KOH and 8.5 wt. % urea. Then, the reaction mixtures were maintained at -30 °C until complete freezing, followed by a thawing step at 20 °C under vigorous agitation, until a clear and transparent solution of Cs was obtained. After removal of air bubbles by centrifugation at 5000 ×g for 15 min at 4 °C, the prepared solutions were maintained at 60 °C for 1 h (solvent evaporation technique), promoting the formation of Cs physical gels. After exhaustive washing with Milli-Q water, to remove the residual alkali/urea solution, prepared hydrogels were immersed in an ethanol solution (100%) for 3 days to improve the resistance of the gels [24].

Foremost, Cs-based hydrogels with different AD and Mw were prepared at a concentration of 3% (w/v) [24], to study the effect of these two parameters on the structural, mechanical and rheological features of elaborated hydrogels. The corresponding code to each hydrogel was recorded in **Table S2**. Subsequently, an optimization of the ideal concentration for the formation of Cs-based hydrogels was performed. Accordingly, different concentrations were used, namely 1%, 2%, 3%, 4% and 5% of Cs, and the obtained hydrogels were characterized.

### 2.4. Blue crab chitosan rheological behavior in the alkali/urea aqueous solution

To study the stability of the Cs in alkali/urea system, hydrogels (15 mm of diameter × 1 mm of thickness) rheological and gelation behaviors were investigated with dynamic viscoelastic measurements. For all the experiments, a rheometer apparatus (Physica MCR, Anton Paar, GmbH, France) equipped with a plate-plate measuring geometry (25 mm diameter, 0.1 mm gap) was used. Oscillatory measurements of the storage modulus ( $G'$ ) and loss modulus ( $G''$ ) were carried out under a strain sweep from 0.1% to 1000% at 37 °C with a frequency of 1



Hz. Thermo-viscoelasticity properties in a ramp temperature from 20 to 80 °C was investigated, under constant frequency (1 Hz) and strain (1%), at a heating rate of 2 °C/min. A solvent trap was applied to prevent water evaporation when heating. The data were analyzed with Rheoplus software from Anton Paar.

## **2.5. Analytical methods**

### **2.5.1. Hydrogels microstructure**

The cross-section of Cs-based hydrogels was studied using scanning electron microscopy SEM (Hitachi S4800), at an angle of 90° to the surface, at different magnifications. Prior to imaging their cross-section, hydrogel samples were lyophilized, sectioned and fixed on the SEM support using double side adhesive tape, and observed up to a 2000 x magnification, under an accelerating voltage of 2.0 kV and an absolute pressure of 60 Pa, after being sputter coated with a 5 nm thick gold.

### **2.5.2. Moisture content of Cs-based hydrogels**

The water content was determined according to the methods described by AOAC (2000) [25]. The water content of the elaborated hydrogels was measured, in triplicate, by drying about 100 mg of each sample in an oven at 105 °C until the dry weight of the sample was reached (constant weight). Weights before and after drying were measured. The moisture content of hydrogels was determined by measuring the mass loss of each film in triplicate and expressed as follows:

$$MC (\%) = \frac{W_0 - W_1}{W_0} \times 100$$

where  $W_0$  and  $W_1$  are the respective masses (g) of hydrogels before and after drying at 105 °C.

### **2.5.3. Swelling rate of hydrogels**

The swelling test was performed on pieces of hydrogels with masses of 20-30 mg. The samples were immersed in phosphate-buffered saline (PBS) at 37 °C and after 24 h of

incubation, the samples were removed, oven-dried and the masses were measured again [26].

The swelling rate (SR), repeated three times, was calculated as follows:

$$SR (\%) = \frac{M_s - M_d}{M_d} \times 100$$

where SR is the swelling rate (%),  $M_d$  is the mass (g) of the oven-dried hydrogel and  $M_s$  is the mass (g) of the swollen hydrogel.

#### 2.5.4. Infrared spectroscopy analyses

The prepared Cs-based hydrogels FT-IR analysis was performed by means of a spectrometer (Agilent Technologies, Carry630 series) with an attenuated reflection accessory (ATR) containing a diamond/ZnSe crystal, at room temperature (25 °C). Spectra were recorded in the spectral range frequencies of 650-4000  $\text{cm}^{-1}$ , with 32 scans of interferograms and a resolution of 4  $\text{cm}^{-1}$ . Prior to analysis, FT-IR spectrometer was calibrated via a background spectrum recorded from the clean and empty diamond for each spectrum. Data analysis and treatment were carried out using the OMNIC Spectra software (ThermoFisher Scientific).

#### 2.5.5. X-ray diffraction studies

To further investigate the structural characteristics of the prepared hydrogels, XRD patterns were recorded using an X-ray diffractometer (D8, Advance Bruker XRD diffractometer, Germany). Ni-filtered Cu  $K\alpha$  radiation ( $\lambda = 1.5406 \text{ \AA}$ ) was used to record the X-ray patterns. The relative intensity was recorded in the scattering range  $2\theta$  of 5–50° with a step size of 0.02° and a counting time of 5 s/step, with an error of  $\pm 1^\circ$ .

#### 2.5.6. Thermal properties of blue crab chitosan-based hydrogels

Thermogravimetric analysis (TGA Q500 High Resolution, TA Instruments), operating under nitrogen flow, was used to study the thermal stability of Cs-based hydrogels. The mass change of a sample as a function of temperature augmentation is the basis of TGA, and the progressive change in mass (%) as function of temperature, is recorded. Cs-based hydrogels,

initially about 4 mg, were heated from 25 to 700 °C at a heating rate of 20 °C/min and constantly measured with an accuracy of 0.01 mg. Cs-based hydrogel thermograms were subsequently analyzed using TA Universal V4.5A software.

### 2.5.7. Evaluation of hydrogels mechanical properties

Hydrogel compression tests were carried out using the DMA50 (Dynamic Mechanical Analyzer) universal testing machine (Metravib, Brand of ACOEM, France) at a temperature of 25 °C and a compression speed of 1 mm/min. Samples were compressed at 10%, 20%, 30%, 40%, 50% and 60%, and then reverted at the same speed of 1 mm/min, to obtain the stress-strain curves for gels' compression-recovery. The dimensions of the hydrogel specimens (parallelepiped) for compression tests were 10 mm × 5 mm × 5 mm (based on the apparatus requirements). The stress-strain curve hysteresis was recorded and treated by the instrument software.

### 2.5.8. Hydrogels *in vitro* degradation test

Cs-based hydrogels *in vitro* biodegradation study was monitored through the gravimetric method described by Qu *et al.* [27]. Briefly, hydrogels (approximately 100 mg) were immersed in 10 ml of phosphate buffer saline (PBS) at pH 7.4 (physiological microenvironment simulation) and pH 5.5 (acidic microenvironment), at 37 °C and under gentle shaking (approximately 100 rpm). Thereafter, hydrogel samples were removed, at each desired interval time, washed with Milli-Q water to remove the excess of salinity, oven-dried for 48 h at 60 °C and then weighed. The remaining weight of hydrogels (%) was calculated based on the following equation:

$$\text{Remaining weight ratio (\%)} = \frac{M_t}{M_i} \times 100$$

where  $M_t$  is the remaining hydrogels dry weight after degradation at each selected time interval and  $M_i$  is the initial hydrogels dry weight.

## 2.6. *In vitro* riboflavin loading and release kinetics

The amount of riboflavin incorporated in hydrogels was studied. Briefly, wet Cs-based hydrogel (30 mg) were suspended in 10 ml of riboflavin solution (1-5 g/l) in dark at 5 °C for 48 h. The riboflavin entrapment efficiency and loading capacity by the hydrogels were determined considering the derivative thermogravimetric (DTG) thermograms [28], by subtracting the amount of riboflavin in the supernatant from the total amount applied [24]:

$$\text{Riboflavin loading capacity (\%)} = \frac{\text{Mass of loaded riboflavin}}{\text{Mass of hydrogel samples}} \times 100$$

$$\text{Riboflavin entrapment efficiency (\%)} = \frac{\text{Mass of loaded riboflavin}}{\text{Mass of initial riboflavin}} \times 100$$

Regarding the riboflavin release studies, loaded hydrogel samples (30 mg) were subsequently incubated in 10 ml of aqueous HCl and NaCl (0.1 M) with different pH values (pH 2.0, 4.5 and 7.4) at 37 °C, with stirring. At each time interval, an aliquot of the supernatant (2.5 ml) was withdrawn and replaced by fresh medium at the same volume. The amount of released riboflavin was determined spectrophotometrically, considering the cumulative amount of riboflavin in each of the release system. The amount of riboflavin was estimated using a UV-visible spectrometer (Agilent Technologies, Carry 630 series) at 450 nm on the basis of a riboflavin calibration curve (**Data not shown**). All studies were performed in duplicate and the average values were reported.

## 2.7. Statistical analysis

Statistical analyses were performed with SPSS ver. 17.0, professional edition (SPSS, Inc., Chicago, IL, USA) using ANOVA analysis at a p-value < 0.05. A standard deviation at the 95% confidence level was used to compare all parameters analyzed for the different hydrogels. All assessments were repeated three times and average values with standard deviation errors were reported.

### 3. Results and Discussion

#### 3.1. Microstructure analysis of Cs-based hydrogels

Since understanding biomaterials functional properties is based on their structure knowledge, the examination of Cs-based hydrogels microstructure, reflecting polymer and molecules interactions, is required [29].

SEM images showing the pore microstructure (cross section) of Cs-based hydrogels, with different AD and Mw, are displayed in **Fig. 1**. The pore size of the prepared hydrogels changed in the range of 1 ~ 6  $\mu\text{m}$  and became bigger and bigger as the Cs AD increased, with more compact distribution. For example, pore size values of ~ 1  $\mu\text{m}$  for CsIII-0 based hydrogel (**Fig. 1G**), 2  $\mu\text{m}$  for CsII-0 based hydrogel (**Fig. 1D**) and 3  $\mu\text{m}$  for CsI-0 based hydrogel (**Fig. 1A**) were reached, suggesting that lower AD allowed the preparation of a more well-organized network structure, which could contribute to mechanical support [30].

It was found likewise that the hydrogel pore size had the tendency to decrease with the increase of Cs Mw. Indeed, the pore size (approximately 4  $\mu\text{m}$ ; **Fig. 1I**) of CsIII-3 based hydrogel, showing a microstructure, filled with larger interconnected pores, was about twice of that for CsIII-1 based hydrogel (approximately 2  $\mu\text{m}$ ; **Fig. 1H**), which could lead to modulations in Cs-based hydrogels swelling and drug release behaviors [17].

In another aspect, overall Cs-based hydrogels, regardless Cs AD and Mw, as shown in **Fig. 1**, the formed hydrogels network revealed a uniformly distributed porous three-dimensional architecture, with, to variable extend, a roughness matrix surface. The pores interconnected in a recurrent style inside the hydrogels network affords a suitable medium flow and drug transport channels, being therefore appropriate for drug delivery [26,31].

#### 3.2. Hydrogels moisture content determination

Moisture content (MC) of Cs-based hydrogels, reported in **Table 1**, revealed that values decreased with the decrease of the AD, reaching 82%, 81% and 79%, for CsI-0 (AD=17%),

CsII-0 (AD=13%) and CsIII-0 (AD=8%) based hydrogels, respectively ( $p<0.05$ ). however, considering Cs Mw, MC values were found to be strengthened with the decrease of Cs Mw. Indeed, regarding an AD of 8% (CsIII), hydrogels MC rates of 79.90%, 80.26% and 81.83% were reached with respective Mws of 115 kDa (CsIII-0), 78.43 kDa (CsIII-1) and 16.04 kDa (CsIII-3), probably due a decrease of crosslinking density [5]. In fact, hydrogels are systems known for their remarkable water-holding capacity during their preparation, and the water content is one of the most features that distinguishes hydrogels from other biomaterials. Their water-rich structure facilitates, indeed, the transport of nutrients and molecules between the external environment and the hydrogel, which allows to mimic the function of cells in the body [9].

Consequently, it could be proposed that the increase of CS MW, besides the decrease of its AD, as well as Cs-based hydrogels soaking in ethanol solution (100%), allowed the decrease in Cs-based hydrogels water content, and thereby, reducing pore sizes [24], which was consistent with SEM data. This finding seems to be beneficial for Cs-based hydrogels mechanical properties enhancement.

### 3.3. Evaluation of Cs-based hydrogels swelling properties

As an absorbent matrix, the degree of swelling of a hydrogel is a key parameter that is closely related to the ability of hydrogels to release active ingredients [32]. Swelling is defined as a continuous transition process from the solvent-free glassy state or partially rubbery state to a relaxed rubbery solvent containing state. The solvent infiltration and the elastic contraction from the network strain, as two opposite forces, create a skirmish in the swelling process, which reaches the equilibrium, when they reach a dynamic balance [33]. In this context, the effect of Cs AD and Mw on Cs-based hydrogels swelling ratio (SR) was studied and results are recorded in **Table 1**.

Results display that Cs-based hydrogels water absorption capacity was found to be dependent to the Cs AD and Mw. Indeed, SR values increased with the decrease of Cs AD as well as the decrease in its Mw. For example, hydrogels developed with CsI (CsI-0; AD=17%) exhibited SR value of  $13.59 \pm 0.45$  g/g, compared to CsIII-0 based hydrogel, prepared with lower AD Cs (CsIII-0; AD=8%), with SR exceeding 18 g/g (**Table 1**). Moreover, regarding CsIII-based hydrogel, respective SR values of more than 18 g/g, 22 g/g and 26 g/g were reached with hydrogels prepared with GCsIII-0 (115 kDa), GCsIII-1 (78.43 kDa) and CsIII-3 (16.04 kDa).

It is well known that the swelling properties of hydrogels depend on the hydrophilic nature of polymeric chains and the nature of bonds inside the matrix structure. Thus, it is possible to deduce that the decrease of Cs AD, and thereby, the increase of the  $-NH_2$  groups number, allowed the improvement of the hydrophilicity of the elaborated hydrogels, favoring their interaction with water molecules [34,35]. In addition to the polarity of the hydrogels, the degree of crosslinking and hydrogels porosity were found to well correlate with the ability of Cs-based hydrogels to absorb water [12,27].

### 3.4. Hydrogels spectroscopic characterizations

#### 3.4.1. FT-IR analysis

The FT-IR spectra of Cs-based hydrogels were shown in **Fig. 2**. Compared to the polymer powder [21], characteristic Cs absorption bands at  $3417\text{ cm}^{-1}$ ,  $1627\text{ cm}^{-1}$ ,  $1544\text{ cm}^{-1}$ ,  $1407\text{ cm}^{-1}$  and  $1020\text{--}1097\text{ cm}^{-1}$  linked to the  $-OH$ , amide I groups ( $-C=O$ ), amide II ( $-NH_2$ ),  $-CH$  and glycoside rings, respectively, were noted to be rearranged. Indeed, the  $N-H$  peak in the FT-IR spectra of the Cs-based hydrogels was found to be shifted significantly to higher wavenumbers overlapping with the peak of the  $O-H$  stretching vibrations. The peak at  $3500\text{--}3200\text{ cm}^{-1}$  straitened, and revealed the tendency to break into several small peaks, demonstrating the weakening of the inter- and intra-molecular hydrogen bonds and the occurrence of some reactions on the two groups [34-39].

The peak of the amide I group weakened remarkably and almost disappeared, indicating that concentrated alkali has reacted with the acetyl amino group of Cs [38,39]. Moreover, new stretch vibration absorption bonds appeared at about  $3264\text{ cm}^{-1}$ ,  $2500\text{ cm}^{-1}$  and  $785\text{ cm}^{-1}$ , indicating that the alkali/urea aqueous solvent affected the structure of Cs to some extent. Indeed, active hydroxyl group of Cs reacted with the concentrated alkali, leading thereby to the destruction of the native hydrogen bonds of Cs effectively and making Cs highly swell or even dissolve in the alkali solution.

These findings confirmed further during the dissolution process, alkali not only reacts with the hydroxyl group, but also with the acetyl amino group of Cs, leading to the weakening of the amide I peak ascribed to acetyl amino group [40,41]. Moreover, The FT-IR spectra of all Cs-based hydrogels are quite similar, regardless Cs AD and Mw, accounting for the stability of Cs in the alkali/urea aqueous solution system [24, 42,43].

### 3.4.2. XRD patterns study

To further clarify the structural changes in the Cs matrix, during dissolution in the alkali/urea aqueous system and gelling, and regarding the effects of Cs Mw and AD, XRD patterns of Cs-based hydrogels were studied and compared to the polymer powder profiles (**Fig. 3**). X-diffractograms of Cs-based hydrogels revealed marked differences in the molecular state. Indeed, diffraction peaks nearby  $13.1^\circ$  and  $21.3^\circ$ , attributed to (020) and (110) planes of Cs, respectively, were detected, reflecting the semi-crystalline structure of Cs [21,44]. The major peaks at  $2\theta = 37.7^\circ$ ,  $34.32^\circ$ ,  $32.4^\circ$  and  $28.9^\circ$  observed in the X-diffractograms could be attributed to the alkali (LiOH) used for the dissolution of Cs [45].

As shown in **Fig. 3**, the Cs-based hydrogels displayed the characteristic diffraction patterns of both Cs and alkali at the same time. However, the crystallinity of the physical Cs-based hydrogels clearly diminished in comparison with that of Cs powder, where the above mentioned initial characteristic peaks became broader and weaker, depending on Cs AD and



Mw. In fact, convenient with the SEM images, the crystallinity of Cs-based hydrogels decreased with the increase of Cs AD (CsI-0 based hydrogel) and the decrease in its Mw (Cs-1 and Cs-3 based hydrogels), suggesting a transition from a crystalline structure to an amorphous state during the dissolution and the gelling process [46,47]. This result strongly confirmed that Cs solubility was related to its crystallinity.

With the aid of alkali solution and the freezing to -30 °C, water molecules diffuse in the Cs macromolecular chain. The subsequent thawing and stirring steps during hydrogels preparation process are beneficial for the dissolution of Cs, as the intra- and inter-molecular hydrogen bonds of Cs would be broken during dissolution, leading to the loss of crystallinity [48,49].

The dissolution of Cs in the alkali aqueous system begins at the amorphous side with a loose structure at first, and afterwards reaches the crystal zone with a rather thicker construction and low temperature. This exhibits a crucial role in the Cs crystalline configuration destruction [26,50]. Meanwhile, overall findings proposed that the chemical structure of Cs was relatively stable in the alkali/urea aqueous solution [5,24].

### 3.5. Cs AD and Mw affected based hydrogels thermal properties

Thermal stability/degradation behavior of Cs-based hydrogels, with respect to their AD and Mw, was studied, and results in terms of TGA and derivate (DTG) thermograms, are shown in **Supplementary data Fig. S1**. The thermal decomposition data in terms of the corresponding degradation temperatures, the weight loss ( $\Delta w$ ) and the residue (**R**), were estimated (**Table 2**).

Based on data from the obtained TGA thermograms, the thermal decomposition profiles of the overall Cs-based hydrogels exhibited a similar weight loss process in the temperature range of 20–800 °C, indicating the polymer pyrolysis, and characterized by three major phases (**Supplementary data Fig. S1**), typical fingerprint of Cs thermal decomposition [32].

The first phase corresponded to a weight loss of 6% (CsIII-0 based hydrogel) to 19% (CsI-3 based hydrogel), apparently resulted from evaporation of adsorbed water by Cs at a temperature (Td1) range from 28-46 °C to 129-158 °C, reaching its maximum mainly below 130 °C, expect for the CsIII-0 based hydrogel (133.54 °C). The different content of bound and unbound water in the hydrogels could explain the observed difference in onset temperature [51]. Indeed, in line with data from the SEM analysis and results above mentioned, CsIII-0 based hydrogel exhibited higher onset temperature as a result of more strongly bound water, related to a more homogeneous network structure. However, less uniform network with macro-phase separation like structure, observed in hydrogels based on CsI-3, was found to responsible of more unbound water in the based hydrogel structure [28,48].

Considering the DTG curves, the temperature, at which the decomposition process was the shrillest, was revealed by the weight loss peak (**Supplementary data Fig. S1**). In the range the third phase of Cs-based hydrogels pyrolysis process (200-550 °C), where higher  $\Delta W$  were reached, peaks located at temperatures of 268.81, 266.09 and 261.55 °C, were found for the CsI-0, CsI-1 and CsI-3 based hydrogels, respectively, whereas those found at 279.71, 274.26 and 273.35 °C were related to the CsIII-0, CsIII-1 and CsIII-3 based hydrogels, respectively (**Table 2**). Thus, polymers pyrolysis temperature differences are mainly assigned to the macromolecular interaction, crystallinity index, or orientation. The TGA results proved that CsIII-0 based hydrogel was reorganized in more well-ordered network structure, during the dissolution in the alkali/urea system at low temperatures and the regeneration process in ethanol, ensuing a rather high crystallinity and more homogeneous architecture. Finally, residual decomposition reactions leading to the total degradation of the Cs ring in the hydrogels was found to be around 550 °C [52].

Regarding the residual mass (R) of the prepared hydrogels, values were found to decrease with the decrease of the Cs Mw and the increase of its AD, with values of 33.70% (CsI-0 based

hydrogel), 30.59% (CsI-1 based hydrogel) and 29.88% (CsI-3 based hydrogel). Considering CsII-based hydrogels, R values of 34.34%, 33.05% and 29.58% were reached for the CsII-0, CsII-1 and CsII-3 based hydrogels, respectively. R values of 47.69%, 40.53% and 38.68% were noted for CsIII-0, CsIII-1 and CsIII-3 based hydrogels, respectively (**Table 2**). Accordingly, it could be concluded that the thermal stability of the Cs-based hydrogels is positively correlated with its AD and disproportionate to its Mw. Moreover, as discussed earlier, TGA findings confirmed that the increased stability of the Cs-based hydrogels was due to increasing macromolecular chains crosslinking [28,32].

### 3.6. Hydrogels mechanical properties as affected by Cs structural parameters

#### 3.6.1. Rheological behavior

The rheological properties of Cs-based hydrogels, storage modulus ( $G'$ ) and loss modulus ( $G''$ ), were shown as a function of strain at 37 °C (**Fig. 4A-C**). Independently of Cs AD or Mw, Cs-based hydrogels displayed higher elastic behavior ( $G' > G''$ ) than the viscous behavior ( $G' < G''$ ), suggesting a distinctive feature of a strong hydrogel.

Since the elasticity of the sample, defined as the stored energy due to the elastic deformation, is reflected by the storage modulus  $G'$ , the higher the  $G'$  value is, the tougher against distortion the hydrogel is [33]. **Fig. 4A-C** shows that for all the Cs-based hydrogel samples, the moduli ( $G'$  and  $G''$ ) fluctuated slightly with deformation in the test strain range of 500%. Comparing the hydrogel samples, for CsIII-0 based hydrogel, the  $G'$  (more than 130 kPa) was found to be significantly higher than that of CsII-0 (more than 82 kPa) and CsI-0 (more than 35 kPa) based hydrogels. Additionally, for CsIII-1 ( $G'$  about 30 kPa) and CsIII-3 ( $G'$  more than 17 kPa) based hydrogels, the  $G'$  values were significantly lower than that of CsIII-0 based hydrogel ( $p < 0.05$ ). The same tendency was detected with the other hydrogels based on CsII (AD of 13%) and GCsI (AD of 17%).

Before hydrolysis,  $G'$  of Cs-based hydrogels, independently of Cs AD, was four times more than the value of Cs-1 and Cs-3 based hydrogels, thus, the creation of a more stable network, leading to a greater maximum storage modulus  $G'$ .

This finding could be mainly assigned to the stronger interactions of Cs macromolecular chains, with high average molecular weight, than medium and lower average molecular weights Cs (Cs-1 and Cs-3, respectively). The formation of covalent bonds between the Cs and the alkali/urea system, allowed thereby remarkably the enlargement of the strength of hydrogels and the enhancement of their mechanical properties [5,27,33].

Data of gradually decreasing storage modulus  $G'$  of the hydrogels, with the decrease of Cs AD and the increase of the Mw, were consistent with the gradually increasing SR results above described (**Table 1**), further, principally ascribed to the progressively hydrogels crosslinking density diminishing [24,53].

As displayed in **Fig. 4A-C**, it is likewise found that an increase in the deformation, more than 500%, was associated with loss/viscous modulus  $G''$  enlargement and storage/elastic modulus  $G'$  decline, as the network movement increased [54], demonstrating that at higher strains elastic flow of the gel network decreased. However, unlike the  $G'$  profile, the gel-sol transition strain value was found not significantly influenced with the Cs AD or Mw.

In another aspect, there was found no remarkable difference of Cs-based hydrogels rheological properties as function of the temperature (**Supplementary data Fig. S2**). Indeed, interestingly, as the temperature increased from 10 to 60 °C, there was no change of  $G'$  and  $G''$  of the hydrogel samples. Therefore, physical Cs-based hydrogels, based on the dissolution in the alkali/urea aqueous system at low temperatures, exhibited stable rheological properties against temperature, regardless the Cs AD or Mw.

Such rheological behaviors of Cs-based hydrogels, with interesting elastic and solid characteristics, showed the attendance of a promising material for tissue engineering application

[55]. Moreover, rapid drug loss prevention and better sustained release properties could be potentially provided by high gel strength and short gelation time of the hydrogel, as obtained with the Cs-based hydrogels [56].

### 3.6.2. Compressive study

Considering the bone tissue engineering, the mechanical properties of biomaterials like hydrogels are design features of priority [57,58]. To have additional insight into the mechanical behavior of Cs-based hydrogels, compressive properties were evaluated by exposing wet gels to compression testing and the stress vs. strain compressive curves, with different Cs ADs and Mws, are shown in **Fig. 4D-F**. Mechanical experimental outcomes display that under compression, the compressive strength of the Cs-based hydrogel samples increased with the increase in compressive strain for all hydrogel formulations. More particularly, the compressive stiffness of Cs-based hydrogels increased concomitantly with the increase of the applied compressive strain in the range of 5-7% deformation, and then stuck to rise but in a slower manner, indicating that the Cs-based hydrogels were sturdy and ductile.

The order of the mechanical properties was found as: CsIII>CsII>CsI. Indeed, when the Cs AD increased from 8% (CsIII based hydrogel) to 17% (CsI based hydrogel), the fracture stress values of the Cs-based hydrogels decreased to 0.35 MPa for CsI-0 based hydrogel, while values of 0.49 MPa and 0.71 MPa were reached with CsII-0 and CsIII-0 based hydrogels, respectively ( $p<0.05$ ). CsIII-3 based hydrogel was found to endure 40% deformation, whereas CsII-3 and CsI-3 based hydrogels were capable to bear only 35% and 30% deformation, respectively, because of the decrease in the physical crosslink density of the Cs network (**Fig. 4D-F**), suggesting a relatively high strength for CsIII based hydrogel, with the highest macromolecular interactions, the most stable network and the smallest pore size [39,59].

In another side, the increase in Cs Mw was found to result in a significant enhancement in ultimate compressive stress and strain of fracture ( $p<0.05$ ). In fact, hydrogels developed

based on low Mw Cs (CsIII-3, CsII-3 and CsI-3) exhibited mechanical stiffness of more than 0.29 and 0.27 and 0.11 MPa, respectively. However, ultimate stress modulus increased by 2 and more than 3-folds for medium (CsIII-2, CsII-2 and CsI-2) and high (CsIII-0, CsII-0 and CsI-0) Mw Cs, respectively (**Fig. 4D-F**). Interestingly, with ADs less than 13% (CsII and CsIII), even with medium Mw, based hydrogels kept the structural integrity and stability without evidences of any sign of fracture and could recover by themselves subsequently to external pressure removal. This finding strongly demonstrated that the synthesized hydrogel exhibited interesting mechanical properties, thanks to stiffer chains resulting in stronger pore wall, allowing gels thereby to undergo more intense external forces and conditions [33,51,57].

These mechanical data were further consistent with the crystallinity results (**Fig. 3**) and the microstructure of the Cs-based hydrogels (**Fig. 1**).

### 3.7. Hydrogels *in vitro* degradation behavior

The degradation behavior, based on the weight loss system, was monitored in PBS at pH values of 7.4 and 5.5 to simulate the physiological and acidic microenvironments, respectively. Significant differences ( $p < 0.05$ ) were observed, in terms of Cs AD and Mw, considering degradation kinetics over 7 days of incubation time (**Fig. 5**). Additionally, the degradation behavior patterns were peculiar after immersion under simulated physiological (pH 7.4) and acidic (pH 5.5) conditions at 37 °C. However, independently of the swelling conditions and Cs characteristics (AD and Mw), more than 75% of the initial mass was preserved (**Fig. 5**).

Independently of Cs characteristics, hydrogels, in PBS of pH 5.5, underwent most quicker degradation, compared to samples immersed in PBS of pH 7.4. For example, CsIII-0 based hydrogel retained about 91% mass in acidic microenvironment (**Fig. 5A**), and more than 95% mass in PBS pH 7.4 (**Fig. 5B**), within 4 days. Qu *et al.* [27], based on the morphology of the hydrogels observed under SEM images, proved that differences in degradation behavior could be ascribed to an increase in pore sizes, which increased significantly after immersion in PBS.

This increase was more pronounced for hydrogels swollen in acidic conditions (PBS of pH 5.5), that in the long term, could quick the degradation of hydrogels, due to protonation of chitosan amino groups. Indeed, pKa value of D-glucosamine residue is about 6.2~7.0. Subsequently, macromolecular chains bonding become brittle, leading to the hydrogel's networks destruction and decomposition.

As expected, Cs-based hydrogels with higher AD and lower Mw exhibited a faster weight loss after immersion in both media (PBS of pH 5.5 and pH 7.4). After incubation for 7 days, the attained mass losses were about 20%, 22% and 25% for CsI-0, CsI-1 and CsI-3 based hydrogels, respectively, while, CsIII based hydrogels still retained more than 80% (CsIII-0), 78% (CsIII-1) and 75% (CsIII-3) of their original weight, under swelling in pH 5.5 PBS, after 7 days of incubation time (**Fig. 5A**). These findings corroborate well and directly with the pore diameters distribution based on the SEM images, the swelling and mechanical behaviors of prepared hydrogels and the observed crystallinity data. These results proposed that Cs-based hydrogels, with good biodegradability and interesting stability in PBS, could exhibit potential and promising application in tissue engineering [12,55,59].

During the last decades, smart biomaterials as oral administrative drug carriers attracted day-by-day the attention of researchers in the biomedical field [60]. Therefore, Cs-based hydrogels developed in the present study could be considered as porous promising pH-sensitive biomaterial, with sufficient space for the diffusion of small molecules and drugs, and exercising drug release management capability.

### **3.8. Optimization of blue crab chitosan concentration for hydrogels construction**

An optimization of the ideal concentration of Cs for the formation of hydrogels was performed on the basis of the compressive property test and storage modulus determination. CsIII-0 based hydrogel was selected for the optimization of Cs concentration study, considering its appropriate structural architecture, swelling behavior and mechanical strength.

Mechanical properties of the different Cs-based physical hydrogels, considering the compression stress-strain diagrams are illustrated in **Fig. 6A**. The application of a compressive force on the hydrogels made it possible to obtain two phases. At low deformation values (around 5%), an elastic (reversible) deformation was observed as a straight line where the deformation was proportional to the stress. Beyond 5%, the stress increased slowly, giving evidence of a plastic deformation (irreversible) occurrence, due to the breaking of the bonds or rearrangement of the structure [12].

As displayed in **Fig. 6A**, hydrogel compressive strength was improved with the increase of Cs concentration from 0.24 MPa for 1% of Cs to more than 0.48 MPa for hydrogel at 4% of Cs. The Cs solution at 1% concentration was found to be not able to form solid physical hydrogel and the hydrogel prepared was too weak to be handled and analyzed, mainly due to the rather low polymer amount. Indeed, the formed hydrogel was fractured under compressive deformation less than 30%. However, hydrogels prepared with more than 2% Cs were already relatively rigid and resistant. Further, data revealed that fracture resistance of all hydrogel samples was found to be Cs concentration dependent, where 2% Cs-based hydrogel tolerated more than 45% of compressive deformation to be fractured, whereas, 50% of compressive deformation was not sufficient to induce hydrogels fracture at more than 3% Cs (**Fig. 6A**). However, 5% Cs-based hydrogel exhibited a significant decrease in the compressive stress to around 0.4 MPa ( $p < 0.05$ ), compared to 3% and 4% Cs-based hydrogels, with an average value of 50 MPa.

In order to further study the influence of Cs concentration on the resulting hydrogels structure, their rheological behavior was investigated. The shear ( $G'$ ) and loss ( $G''$ ) moduli curves of the Cs-based hydrogels as a function of strain were considered in the rheometer dynamic stress environment (**Fig. 6B**).



Profiles displayed that  $G'$  values of Cs-based hydrogels increased with the increase of Cs concentration, with an increasing strain from 0.1% to 1000%. In fact,  $G'$  of Cs 1%-based hydrogel ( $15.9 \times 10^3$  Pa) at 100% strain was 11.3 times lower than that of Cs 4%-based hydrogel ( $181 \times 10^3$  Pa). Although, in all cases, the storage modulus  $G'$  was below the loss modulus  $G''$ , indicating a predominantly gel-like behavior, the storage modulus  $G'$  decreased significantly ( $p < 0.05$ ), reaching  $63.2 \times 10^3$  Pa, for higher concentration of Cs (5%). In another aspect, 1% Cs-based hydrogel was found to be able to support only around 123% deformation and maintain the gel-like behavior (the point at which  $G'' > G'$ ), while 3% and 4% Cs-based hydrogels were capable to bear more than 574% and 491% deformation, respectively. However, at higher Cs content, the gel structure was kept only at strains below 185% (**Fig. 6B**).

Consequently, from the mechanical and rheological testing data, 3% Cs-based hydrogel exhibited better rheological properties than those of 2% Cs, and the fracture deformation was greater than that of 5% Cs. Similarly, excessive Cs concentration led to thicker and too rigid hydrogel, which could be attributed to chains entanglements excess, leading to hydrogels brittleness [61]. However, due to the gradually improved number of the hydrogen-bonded crosslink regions between the Cs chains, in a relatively concentrated solution, aggregation and entanglement amongst the Cs macromolecular chains will significantly took place.

Therefore, 3% concentration of chitosan solution was carefully chosen to elaborate Cs-based hydrogels in the following section, for the Riboflavin *in vitro* release study.

### 3.9. Encapsulation of riboflavin, *in vitro* loading and release profiles

Hydrogels structure is characterized by three major parameters, namely the volume fraction of polymer in the inflated state, the average molecular weight of based polymers as well as the pore size distribution of the network [9-10]. This architecture of hydrogels allows the diffusion of molecules of different sizes in the network, which makes these biomaterials interesting for drug release applications [7,12].

As the model drug, the kinetics of riboflavin release, through the Cs-based hydrogels were monitored based on the cumulative amounts of released riboflavin as a function of time. Different concentrations of riboflavin (1-5 g/l) were used to investigate the influence of drug concentration on EE and release profiles.

The EE and LC of Cs-hydrogels for riboflavin, as reported in **Table 3**, were found to be drug concentration-dependent ( $p < 0.05$ ). Indeed, the EE values increased from more than 75% for 1 g/l of riboflavin to about 85% for 3 g/l of riboflavin. However, above 3 g/l of riboflavin, the EE dropped dramatically to 68% and 56%, for 4 g/l and 5 g/l of riboflavin, respectively. Regarding the LC of riboflavin, values increased concomitantly with the increase of drug concentration from 24% for 1 g/l of riboflavin to the saturated capacity of 37% at 3 g/l of riboflavin ( $p < 0.05$ ). No significant differences in the riboflavin LC values was noted beyond 3 g/l of riboflavin ( $p \geq 0.05$ ). The decrease in the amount of encapsulated riboflavin at high concentration could be related to the saturation of hydrogel (limitation of riboflavin loading into Cs-based hydrogel), since the encapsulation of riboflavin was monitored through its diffusion in the hydrogel network.

Riboflavin release profiles from Cs-based hydrogels, at 37 °C, in HCl-NaOH (0.1 M), pH 5.5, exhibited deliverance patterns, characterized by an initial short-time rapid release, during the first 8 h, followed by low riboflavin release to 72 h. Beyond 72 h, the rate of released riboflavin tended to stabilize (**Fig. 7**). Data reveal that hydrogel with lower riboflavin charge showed high initial release in terms of percentage. Indeed, at a riboflavin concentration of 1 g/l, the initial release rate (after 4 h) was 11% relative to the amount of initial riboflavin loaded in the hydrogel. It was of 46% and 79%, after 24 h and at the end of the study (96 h). Regarding a concentration of 5 g/l, the release of riboflavin was 5%, 18% and 36%, after 4 h, 24 h and 96 h, respectively. In terms of the total mass of riboflavin released, the hydrogel group with higher charge released more riboflavin. For example, at a riboflavin concentration of 1 g/l, the amount

released riboflavin was 790 mg after 96 h, while for the 5 g/l riboflavin hydrogel group, about 2 g of riboflavin were released (**Fig. 7A**). This finding could be assigned to the concentration gradient phenomenon as diffusion management force. The more Riboflavin loading increased, the higher concentration gradient increased [27].

The riboflavin (3 g/l) release patterns were further investigated in HCl-NaCl (0.1 M) under different pH conditions (pH 2.0, pH 4.5 and pH 7.4). Deliverance curves, as reported in **Fig. 7B**, showed that riboflavin was barely released from the Cs-based hydrogels, at pH 7.4, of only 13% after 4 days of incubation. However, high amounts of riboflavin were released in acidic pH ( $p < 0.05$ ), further, the amount of released riboflavin from Cs-based hydrogels was higher in pH than pH 4.5 in pH 2.0. Indeed, 16% and 38% of riboflavin were released from Cs-based hydrogel, after 8 h, at pH 4.5 and pH 2.0, respectively. Therefore, Cs-hydrogels were found to release significantly more riboflavin in acidic microenvironments, probably due to higher swelling rates or exhaustive hydrogels structure destruction and thereby faster degradation and release of riboflavin [26,59,60].

#### 4. Conclusion

Different Cs-based hydrogels were successfully engineered, considering Cs AD and Mw, based on the alkali/urea aqueous system following the freezing/thawing/solvent evaporation approach. As expected, hydrogels pore size distribution, mechanical strength, swelling and thermal resistance behaviors besides the *in vitro* biodegradation patterns, were extremely depending on Cs structural characteristics. Low AD coupled with high Mw seemed to be very interesting for the development of promoting biomaterials with stable and appropriate features.

Moreover, Cs-based hydrogels were monitored to study the *in vitro* release of riboflavin selected as the model drug. The obtained release patterns displayed that Cs-based hydrogels could be applied as smart pH-sensitive carrier for drug-controlled release for further biomedical applications (antitumor, protein and peptide, gene and antibiotic drug delivery). Additionally,

due to its suitable structural architecture, swelling behavior and mechanical strength, the application of Cs-based hydrogels seems to be a very interesting alternative in the tissue engineering field.

## Acknowledgement

The present work was funded by the Ministry of Higher Education and Scientific Research, Tunisia.

## References

1. B. Tavsanlı, O. Okay. Mechanically Robust and Stretchable Silk/hyaluronic Acid Hydrogels. *Carbohydr. Polym* 2019, 208, 413-420.
2. M. Khan, J.T. Koivisto, T.I. Hukka, M. Hokka, M. Kellomäki. Composite Hydrogels Using Bioinspired Approach With In Situ Fast Gelation and Self-healing Ability as Future Injectable Biomaterial. *ACS Appl. Mater. Interfaces* 2018, 10, 11950-11960.
3. N. Martin, G. Youssef. Dynamic Properties of Hydrogels and Fiber-reinforced Hydrogels. *J. Mech. Behav. Biomed. Mater* 2018, 85, 194-200.
4. S. Ma, B. Yu, X. Pei, F. Zhou. Structural Hydrogels. *Polymer* 2016, 98, 516-535.
5. J. Duan, X. Liang, Y. Cao, Se. Wang, Zhang, L. High Strength Chitosan Hydrogels with Biocompatibility via New Avenue Based on Constructing Nanofibrous Architecture. *Macromolecules* 2015, 48, 2706-2714.
6. W. Wang, Y. Zhao, H. Yi, T. Chen, S. Kang, T. Zhang, F. Rao, S. Song. Pb(II) Removal from Water Using Porous Hydrogel of Chitosan-2D Montmorillonite. *Int. J. Biol. Macromol* 2019, 128, 85-93.
7. L. Liu, Q. Gao, X. Lu, H. Zhou. In Situ Forming Hydrogels Based on Chitosan for Drug Delivery and Tissue Regeneration. *Asian J. Pharm. Sci* 2016, 11, 673-683.
8. Y.H. Cheng, Y.C. Ko, Y.F. Chang, S.H. Huang, C.J.L. Liu. Thermosensitive Chitosan-gelatin-based Hydrogel Containing Curcumin-loaded Nanoparticles and Latanoprost as a Dual-drug Delivery System for Glaucoma Treatment. *Exp. Eye Res* 2019, 179, 179-187.
9. R. Dimatteo, N.J. Darling, T. Segura. In Situ Forming Injectable Hydrogels for Drug Delivery and Wound Repair. *Adv. Drug Deliv. Rev* 2018, 127, 167-184.
10. T.M. Aminabhavi, S.P. Dharupaneedi. Production of Chitosan-based Hydrogels for Biomedical Applications. *Chitosan Based Biomaterials Volume 1 – Fundamentals* 2017, 295-319.
11. A.M. Slavutsky, M.A. Bertuzzi, Formulation and Characterization of Hydrogel Based on Pectin and Brea Gum. *Int. J. Biol. Macromol* 2019, 123, 784-791.
12. Z. Huang, C. Gao, Y. Huang, X. Zhang, X. Deng, Q. Cai. Injectable polyphosphazene/gelatin hybrid hydrogel for biomedical applications. *Mater. Des* 2008, 160, 1137-1147.



13. Annu, K. Manzoor, S. Ahmad, A. Soundarajan, S. Ikram, S. Ahmed. Chitosan Based Nanomaterials for Biomedical Applications. *Handbook of Nanomaterials for Industrial Applications, Micro and Nano Technologies* 2018, 543-562.
14. B. Choi, S. Kim, B. Lin, B.M. Wu, M. Lee. Cartilaginous Extracellular Matrix-Modified Chitosan Hydrogels for Cartilage Tissue Engineering. *ACS Appl. Mater. Interfaces* 2014, 6, 20110–20121.
15. E. Calo, V.V. Khutoryanskiy. Biomedical Applications of Hydrogels: A Review of Patents and Commercial Products. *Eur. Polym. J* 2015, 65, 252-267.
16. G. Camci-Unal, P. Zorlutuna, A. Khademhosseini. Chapter 4 - Fabrication of Microscale Hydrogels for Tissue Engineering Applications. *Biofabrication, Micro- and Nano-fabrication, Printing, Patterning and Assemblies* 2013, 59-80.
17. S.Z. Md Rasib, H. Md Akil, A. Khan, Z.A.A. Hamid. Controlled Release Studies Through Chitosan-based Hydrogel Synthesized at Different Polymerization Stages. *Int. J. Biol. Macromol* 2019, 128, 531-536.
18. F.A. Fookes, L.N. Mengatto, A. Rigalli, J.A. Luna. Controlled Fluoride Release for Osteoporosis Treatment Using Orally Administered Chitosan Hydrogels. *J. Drug Deliv. Sci. Technol* 2019, 51, 268-275.
19. B. Onat, S. Ulasan, S. Banerjee, E. Erel-Goktepe. Multifunctional Layer-by-layer Modified Chitosan/poly(Ethylene Glycol) Hydrogels. *Eur. Polym. J* 2019, 112, 73-86.
20. K. Saekhor, W. Udomsinprasert, S. Honsawek, W. Tachaboonyakiat. Preparation of an Injectable Modified Chitosan-based Hydrogel Approaching for Bone Tissue Engineering. *Int. J. Biol. Macromol* 2019, 123, 167-173.
21. M. Hamdi, S. Hajji, S. Affes, W. Taktak, H. Maâlej, M. Nasri, R. Nasri. Development of a Controlled Bioconversion Process for The Recovery of Chitosan from Blue Crab (*Portunus segnis*) Exoskeleton. *Food Hydrocoll* 2018, 77, 534-548.
22. S.H. Chang, H.T.V. Lin, G.J. Wu, G.J. Tsai. pH Effects on Solubility, Zeta Potential, And Correlation Between Antibacterial Activity and Molecular Weight of Chitosan. *Carbohydr. Polym* 2015, 134, 74-81.
23. R.Q. Qian, R.W. Glanville. Methods for Purifying Chitosan. *US Patent* 2005, 6896809.
24. B. Huang, M. Liu, C. Zhou. Chitosan Composite Hydrogels Reinforced with Natural Clay Nanotubes. *Carbohydr. Polym* 2017, 175, 689-698.
25. AOAC. Official Methods of Analysis (17th ed.). Washington, DC: *Association of Official Analytical Chemists* 2000.
26. S. Yu, X. Zhang, G. Tan, L. Tian, D. Liu, Y. Liu, X. Yang, W. Pan. A Novel pH-Induced Thermosensitive Hydrogel Composed of Carboxymethyl Chitosan and Poloxamer Cross-Linked by Glutaraldehyde for Ophthalmic Drug Delivery. *Carbohydr. Polym* 2017, 155, 208–217.
27. J. Qu, X. Zhao, P.X. Ma, B. Guo. pH-Responsive Self-Healing Injectable Hydrogel Based On N-Carboxyethyl Chitosan for Hepatocellular Carcinoma Therapy. *Acta Biomater* 2017, 58, 168-180.
28. B. Wang, B. Adhikari, C.J. Barrow. Highly Stable Spray Dried Tuna Oil Powders Encapsulated in Double Shells of Whey Protein Isolate-Agar Gum and Gellan Gum Complex Coacervates. *Powder Technol* 2018, In Press, Corrected Proof.

29. H. Ge, T. Hua, J. Wang. Preparation and Characterization of Poly (Itaconic Acid)-Grafted Crosslinked Chitosan Nanoadsorbent For High Uptake of Hg<sup>2+</sup> And Pb<sup>2+</sup>. *Int. J. Biol. Macromol* 2017, 95, 954-961.
30. A.M. Heimbuck, T.R. Priddy-Arrington, B.J. Sawyer, M.E. Caldorera-Moore. Effects of Post-Processing Methods on Chitosan-Genipin Hydrogel Properties. *Mater. Sci. Eng. C* 2019, 98, 612–618.
31. M.C.G. Pella, M.K. Lima-Tenorio, E.T. Tenorio-Neto, M.R. Guilherme, E.C. Muniz, A.F. Rubira. Chitosan-Based Hydrogels: From Preparation to Biomedical Applications. *Carbohydr. Polym* 2018, 196, 233-245.
32. M.L. Tsai, H.W. Chang, H.C. Yu, Y.S. Lin, Y.D. Tsai. Effect of Chitosan Characteristics and Solution Conditions on Gelation Temperatures of Chitosan/2-Glycerophosphate/Nanosilver Hydrogels. *Carbohydr. Polym* 2011, 84, 1337-1343.
33. F. Wang, Y. Wen, T. Bai. The Composite Hydrogels of Polyvinyl Alcohol–Gellan Gum Ca<sup>2+</sup> With Improved Network Structure and Mechanical Property. *Mater. Sci. Eng. C* 2016, 69, 268–275.
34. B. Ding, H. Gao, J. Song, Y. Li, L. Zhang, X. Cao, M. Xu, J. Cai. Tough and Cell-Compatible Chitosan Physical Hydrogels for Mouse Bone Mesenchymal Stem Cells *in Vitro*. *ACS Appl. Mater. Interfaces* 2016, 10, 19739-19746.
35. Y. Yao, M. Xia, H. Wang, G. Li, H. Shen, G. Ji, Q. Meng, Y. Xie. Preparation and Evaluation of Chitosan-Based Nanogels/Gels for Oral Delivery of Myricetin. *Eur. J. Pharm. Sci* 2016, 91, 144-153.
36. L. Zhang, Y. Li, L. Li, B. Guo, P.X. Ma. Non-Cytotoxic Conductive Carboxymethyl-Chitosan/Aniline Pentamer Hydrogels. *React. Funct. Polym* 2014, 82, 81-88.
37. X. Zhao, P. Li, B. Guo, P.X. Ma. Antibacterial and Conductive Injectable Hydrogels Based on Quaternized Chitosan-Graft-Polyaniline/Oxidized Dextran for Tissue Engineering. *Acta Biomater* 2015, 26, 236-248.
38. C. Chang, S. Chen, L. Zhang. Novel Hydrogels Prepared Via Direct Dissolution of Chitin at Low Temperature: Structure and Biocompatibility. *J. Mater. Chem* 2011, 21, 3865-3872.
39. E. Assaad, M. Maire, S. Lerouge. Injectable Thermosensitive Chitosan Hydrogels with Controlled Gelation Kinetics and Enhanced Mechanical Resistance. *Carbohydr. Polym* 2015, 130, 87–96.
40. Q. Wang, S. Chen, D. Chen. Preparation and Characterization of Chitosan Based Injectable Hydrogels Enhanced by Chitin Nano-Whiskers. *J. Mech. Behav. Biomed. Mater* 2017, 65, 466–477.
41. M. Fan, Q. Hu. Superadsorption Of LiOH Solution on Chitosan as A New Type of Solvent for Chitosan by Freezing/Blasting. *Carbohydr. Polym* 2013, 94, 430– 435.
42. L. Cui, J. Jia, Y. Guo, Y. Liu, P. Zhu. Preparation and Characterization of IPN Hydrogels Composed of Chitosan and Gelatin Cross-Linked by Genipin. *Carbohydr. Polym* 2014, 99, 31-38.
43. X.J. Liu, Y. Chen, Q.L. Huang, W. He, Q.L. Feng, B. Yu. A Novel Thermo-Sensitive Hydrogel Based on Thiolated Chitosan/Hydroxyapatite/Beta-Glycerophosphate. *Carbohydr. Polym* 2014, 110, 62-9.
44. Y. Ogawa, S. Kimura, M. Wada, S. Kuga. Crystal analysis and high-resolution imaging of microfibrillar  $\alpha$ -chitin from *Phaeocystis*. *J. Struct. Biol* 2010, 171, 111–116.

45. N. Vasanthan, I.D. Shin, A.E. Tonelli. Structure, Conformation, And Motions Of Poly(Ethylene Oxide) And Poly(Ethylene Glycol) In Their Urea Inclusion Compounds. *Macromolecules* 1996, 29, 263–267.
46. A.L. Skwarczynska, D. Binias, W. Maniukiewicz, Z. Modrzejewska, T.E.L. Douglas. The Mineralization Effect on Chitosan Hydrogel Structure Containing Collagen and Alkaline Phosphatase. *J. Mol. Struct* 2019, 1187, 86-97.
47. Y. Liu, Z. Liu, W. Pan, Q. Wu. Absorption Behaviors and Structure Changes of Chitin in Alkali Solution. *Carbohydr. Polym* 2008, 72, 235–239.
48. X. Liang, J. Duan, Q. Xu, X. Wei, A. Lu, L. Zhang. Ampholytic Microspheres Constructed from Chitosan and Carrageenan in Alkali/Urea Aqueous Solution for Purification of Various Wastewater. *Chem. Eng. J* 2017, 317, 766-776.
49. H.Y. Zhou, L.J. Jiang, P.P. Cao, J.B. Li, X.G. Chen. Glycerophosphate-Based Chitosan Thermosensitive Hydrogels and Their Biomedical Applications. *Carbohydr. Polym* 2015, 117, 524-53.
50. M.R. Saboktakin, R.M. Tabatabaie, A. Maharramov, M.L. Ramazanov. Synthesis And In Vitro Studies of Biodegradable Thiolated Chitosan Hydrogels for Breast Cancer Therapy. *Int. J. Biol. Macromol* 2011, 48, 747-752.
51. Y. Xie, X. Liao, J. Zhang, F. Yang, Z. Fan. Novel Chitosan Hydrogels Reinforced by Silver Nanoparticles with Ultrahigh Mechanical and High Antibacterial Properties for Accelerating Wound Healing. *Int. J. Biol. Macromol* 2018, 119, 402-412.
52. M.A. Gamiz-González, D.M. Correia, S. Lanceros-Mendez, V. Sencadas, J.L. Gómez Ribelles, A. Vidaurre. Kinetic Study of Thermal Degradation of Chitosan as A Function of Deacetylation Degree. *Carbohydr. Polym* 2017, 167, 52-58.
53. Z. Bao, C. Jiang, Z. Wang, Q. Ji, G. Sun, S. Bi, Y. Liu, X. Chen. The Influence of Solvent Formulations on Thermosensitive Hydroxybutyl Chitosan Hydrogel as A Potential Delivery Matrix for Cell Therapy. *Carbohydr. Polym* 2017, 170, 80-88.
54. J. Maity, S.K. Ray. Removal of Cu (II) Ion from Water Using Sugar Cane Bagasse Cellulose and Gelatin Based Composite Hydrogels. *Int. J. Biol. Macromol* 2016, 97, 238-248.
55. S. Bi, Z. Bao, X. Bai, S. Hu, X. Cheng, X. Chen. Tough Chitosan Hydrogel Based on Purified Regeneration and Alkaline Solvent as Biomaterials for Tissue Engineering Applications. *Int. J. Biol. Macromol* 2017, 104, 224-231.
56. F. Wahid, X.H. Hu, L.Q. Chu, S.R. Jia, Y.Y. Xie, C. Zhong. Development of Bacterial Cellulose/Chitosan Based Semi-Interpenetrating Hydrogels with Improved Mechanical and Antibacterial Properties. *Int. J. Biol. Macromol* 2019, 122, 380-387.
57. Z. Naghizadeh, A. Karkhaneh, A. Khojasteh. Self-Crosslinking Effect of Chitosan and Gelatin on Alginate-Based Hydrogels: Injectable in Situ Forming Scaffolds. *Mater. Sci. Eng. C* 2018, 89, 256-264.
58. C. Chang, M. He, J. Zhou, L. Zhang. Swelling Behaviors of pH- and Salt-Responsive Cellulose-Based Hydrogels. *Macromolecules* 2011, 44, 1642–1648.
59. S. Zang, R. Mu, F. Chen, X. Wei, L. Zhu, B. Han, H. Yu, B. Bi, B. Chen, Q. Wang, L. Jin. Injectable Chitosan/B-Glycerophosphate Hydrogels with Sustained Release Of BMP-7 And Ornidazole In Periodontal Wound Healing of Class III Furcation Defects. *Mater. Sci. Eng. C* 2019, 99, 919-928.



- 1712  
1713  
1714 770 60. Y. Ren, X. Zhao, X. Liang, P.X. Ma, B. Guo. Injectable Hydrogel Based on Quaternized  
1715 771 Chitosan, Gelatin and Dopamine as Localized Drug Delivery System to Treat Parkinson's  
1716 772 Disease. *Int. J. Biol. Macromol* 2017, 105, 1079-1087.  
1717 773 61. D. Zhao, J. Huang, Y. Zhong, K. Li, L. Zhang, J. Cai. High-Strength and High-Toughness  
1718 774 Double-Cross-Linked Cellulose Hydrogels: A New Strategy Using Sequential Chemical and  
1719 775 Physical Cross-Linking. *Adv. Funct. Mater* 2016, 26, 1-9.  
1720  
1721  
1722  
1723  
1724  
1725  
1726  
1727  
1728  
1729  
1730  
1731  
1732  
1733  
1734  
1735  
1736  
1737  
1738  
1739  
1740  
1741  
1742  
1743  
1744  
1745  
1746  
1747  
1748  
1749  
1750  
1751  
1752  
1753  
1754  
1755  
1756  
1757  
1758  
1759  
1760  
1761  
1762  
1763  
1764  
1765  
1766  
1767  
1768  
1769  
1770

## **Figure captions**

**Figure 1:** SEM images of Cs-based hydrogels (GCs) cross sections: GCsI-0 with AD of 17% and Mw of 125.6 kDa (**A**), GCsI-1 with AD of 17% and Mw of 17.8 kDa, (**B**) GCsI-3 with AD of 17% and Mw of 10.44 kDa (**C**), GCsII-0 with AD of 13% and Mw of 118.9 kDa (**D**), GCsII-1 with AD of 13% and Mw of 59.27 kDa (**E**), GCsII-3 with AD of 13% and Mw of 18.54 kDa (**F**), GCsIII-0 with AD of 8% and Mw of 115 kDa (**G**), GCsIII-1 with AD of 8% and Mw of 78.43 kDa (**H**) and GCsIII-3 with AD of 8% and Mw of 16.04 kDa (**I**).

**Figure 2:** ATR-FTIR profiles of Cs-based hydrogels (GCs) with different AD and Mw, (**A**) GCsI, (**B**) GCsII and (**C**) GCsIII, compared to Cs powders spectra.

**Figure 3:** XRD patterns of Cs-based hydrogels (GCs) with different AD and Mw, (**A**) GCsI, (**B**) GCsII and (**C**) GCsIII, compared to Cs powders spectra.

**Figure 4:** Mechanical features of Cs-based hydrogels (GCs) as function of Cs AD and Mw. Rheological behavior (**A**) GCsI, (**B**) GCsII, (**C**) GCsIII,  $f=1$  Hz,  $T=37$  °C. Compressive properties, at a temperature of 25 °C and a compression speed of 1 mm/min, (**D**) GCsI, (**E**) GCsII, (**F**) GCsIII.

**Figure 5:** *In vitro* biodegradation Cs-based hydrogels (GCs) as function of Cs AD and Mw, in PBS at (**A**) pH 5.5 (acidic microenvironment) and (**B**) pH 7.4 (physiological microenvironment simulation), at 37 °C.

**Figure 6:** Mechanical behavior of Cs-based hydrogels as function of Cs concentration. (**A**) Compressive stress vs. compressive strain profiles. (**B**) Viscoelastic properties patterns as function of strain (%),  $f=1$  Hz,  $T=37$  °C.

**Figure 7:** Riboflavin, as the model drug, *in vitro* release profile and kinetics from Cs-based hydrogels. Riboflavin incorporation was monitored by immersion in riboflavin solution (0-5 g/l) in dark at 5 °C for 48 h. The release tests were performed in HCl and NaCl (0.1 M) with different pH values (pH 2.0, pH 4.5 and pH 7.4) at 37 °C. (**A**) Riboflavin release kinetics at different concentrations (0-5 g/l of riboflavin) in pH 5.5. (**B**) Riboflavin (3 g/l) release kinetics at different pH values (pH 2.0, pH 4.5 and pH 7.4).

**Fig. 1**

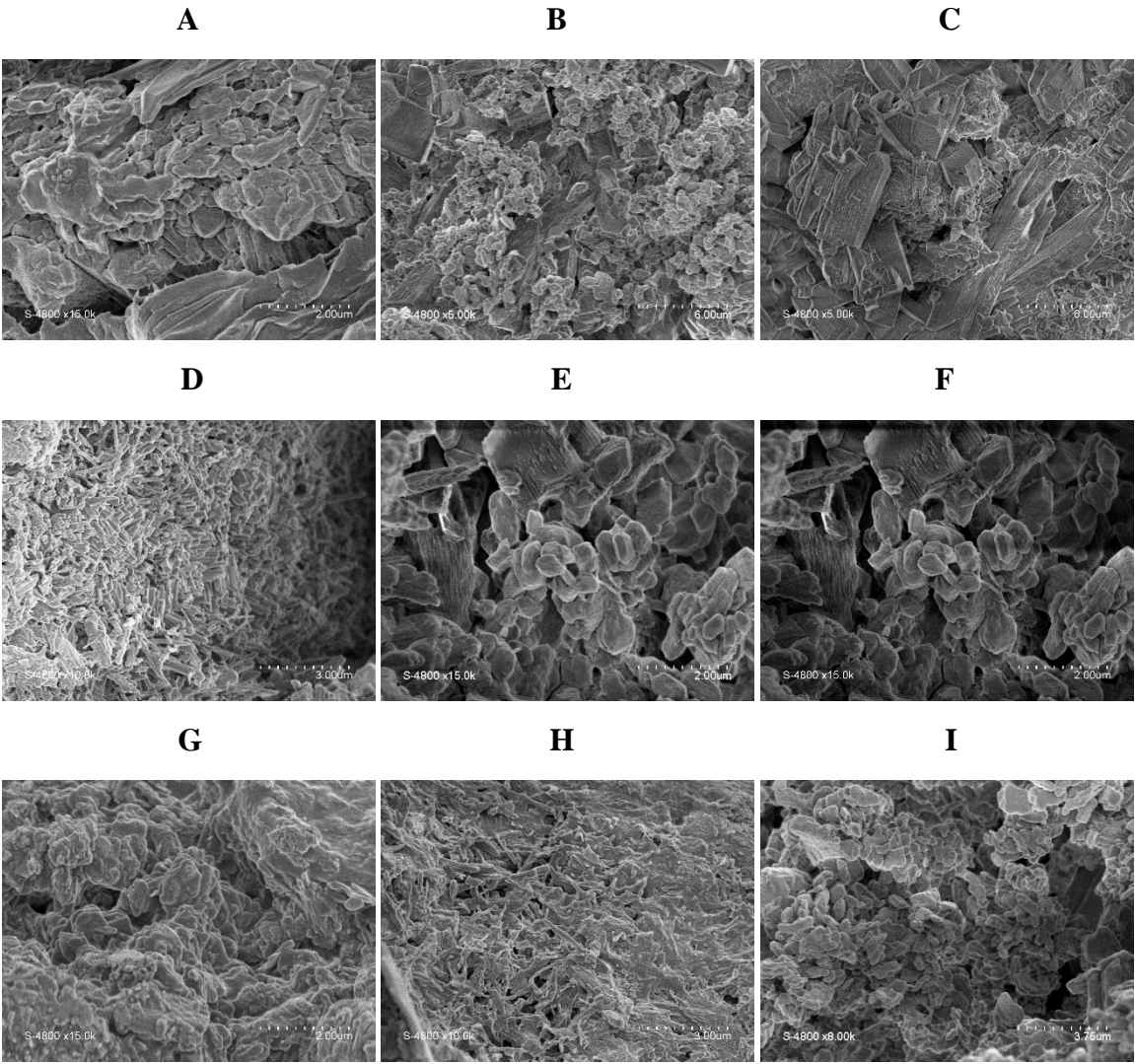


**Fig. 2**

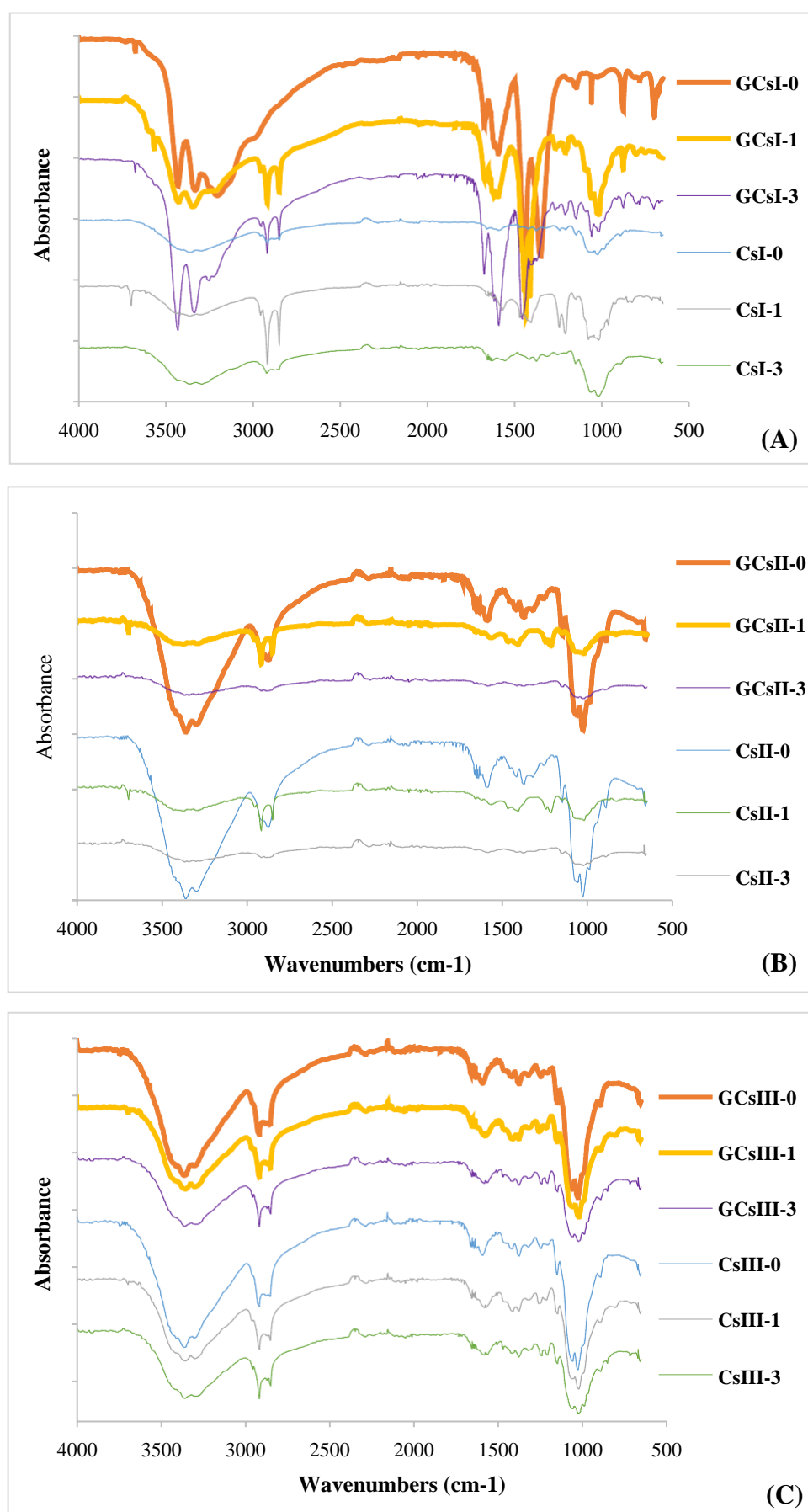


**Fig. 3**

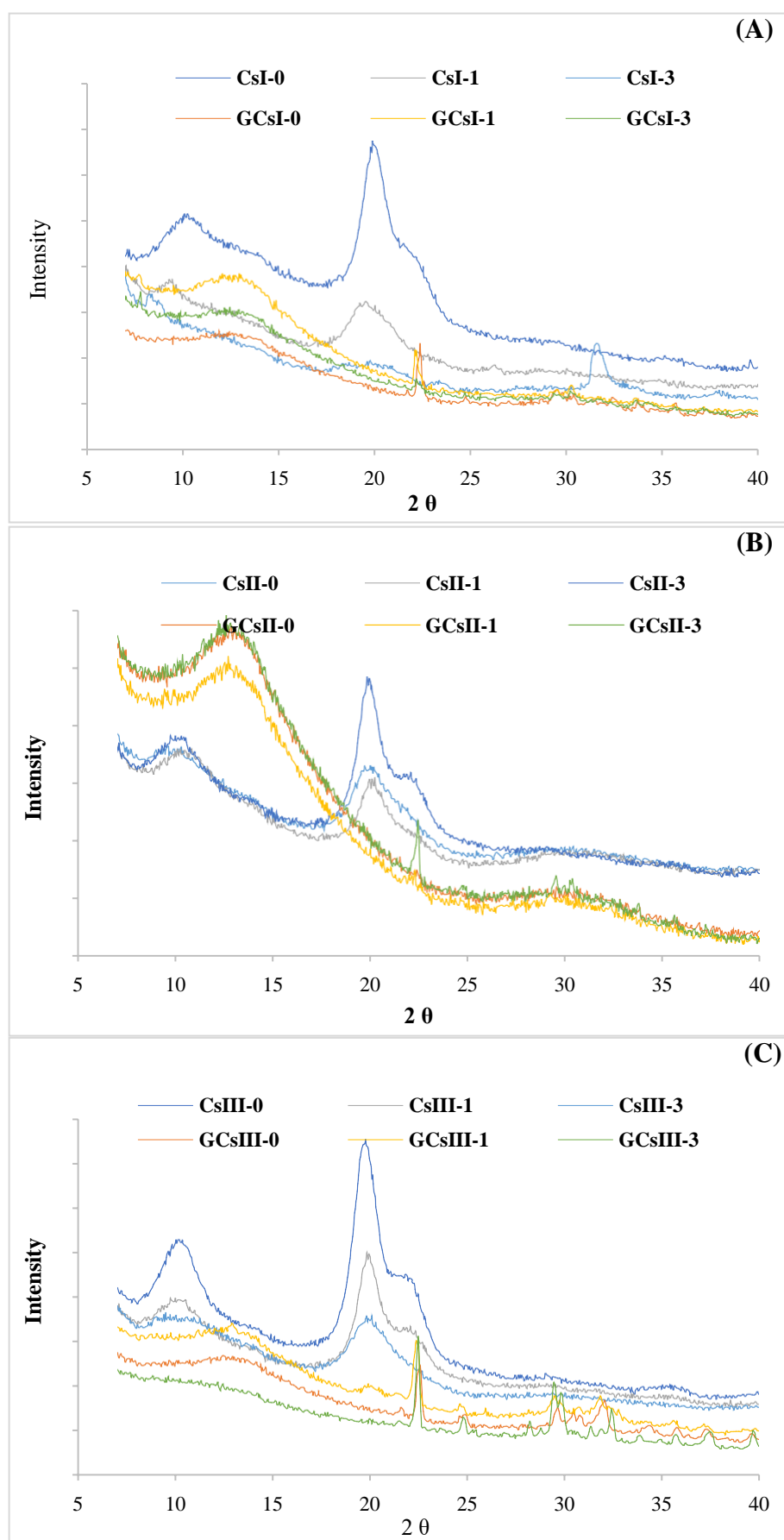


**Fig. 4**

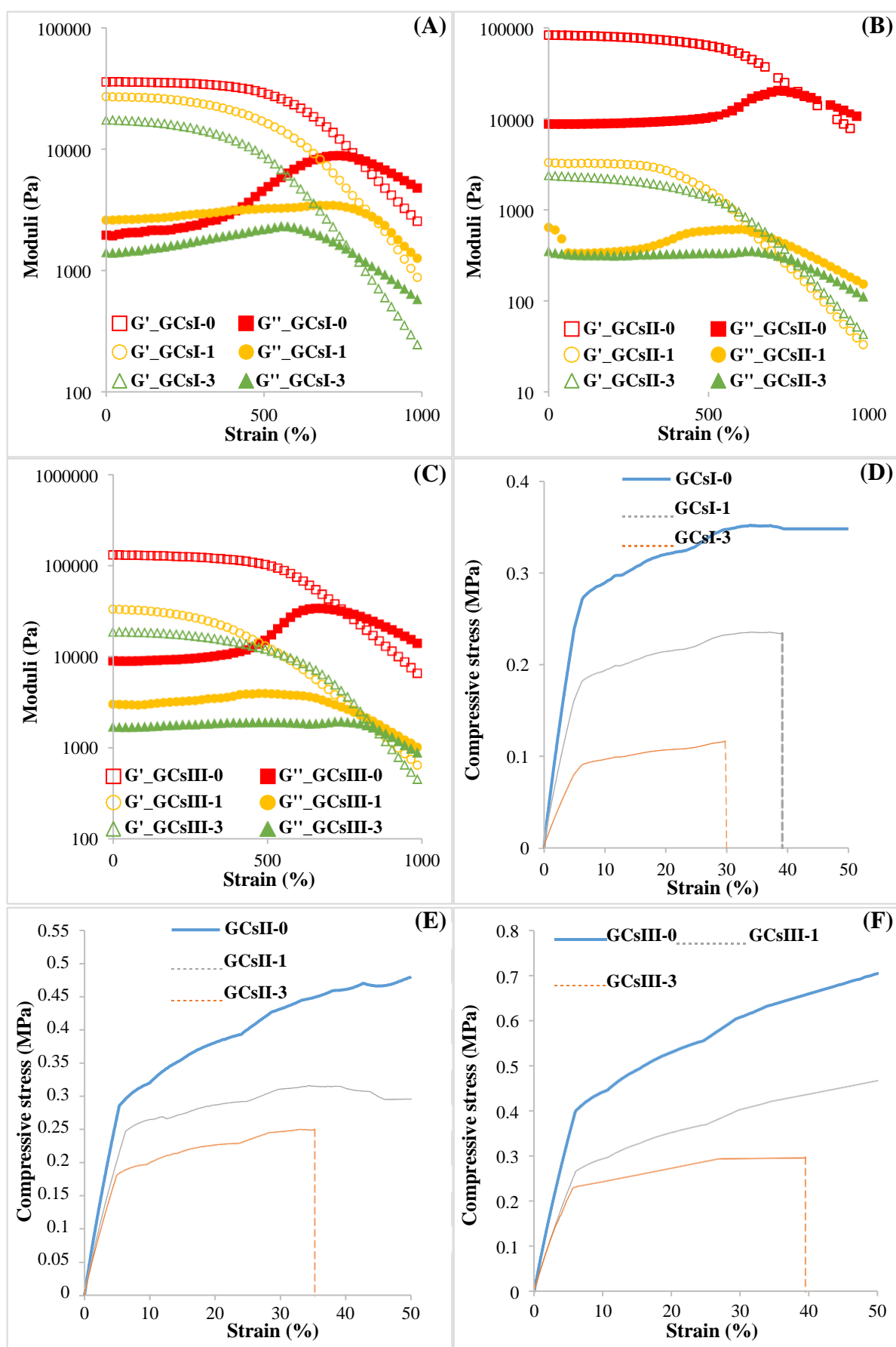


**Fig. 5**

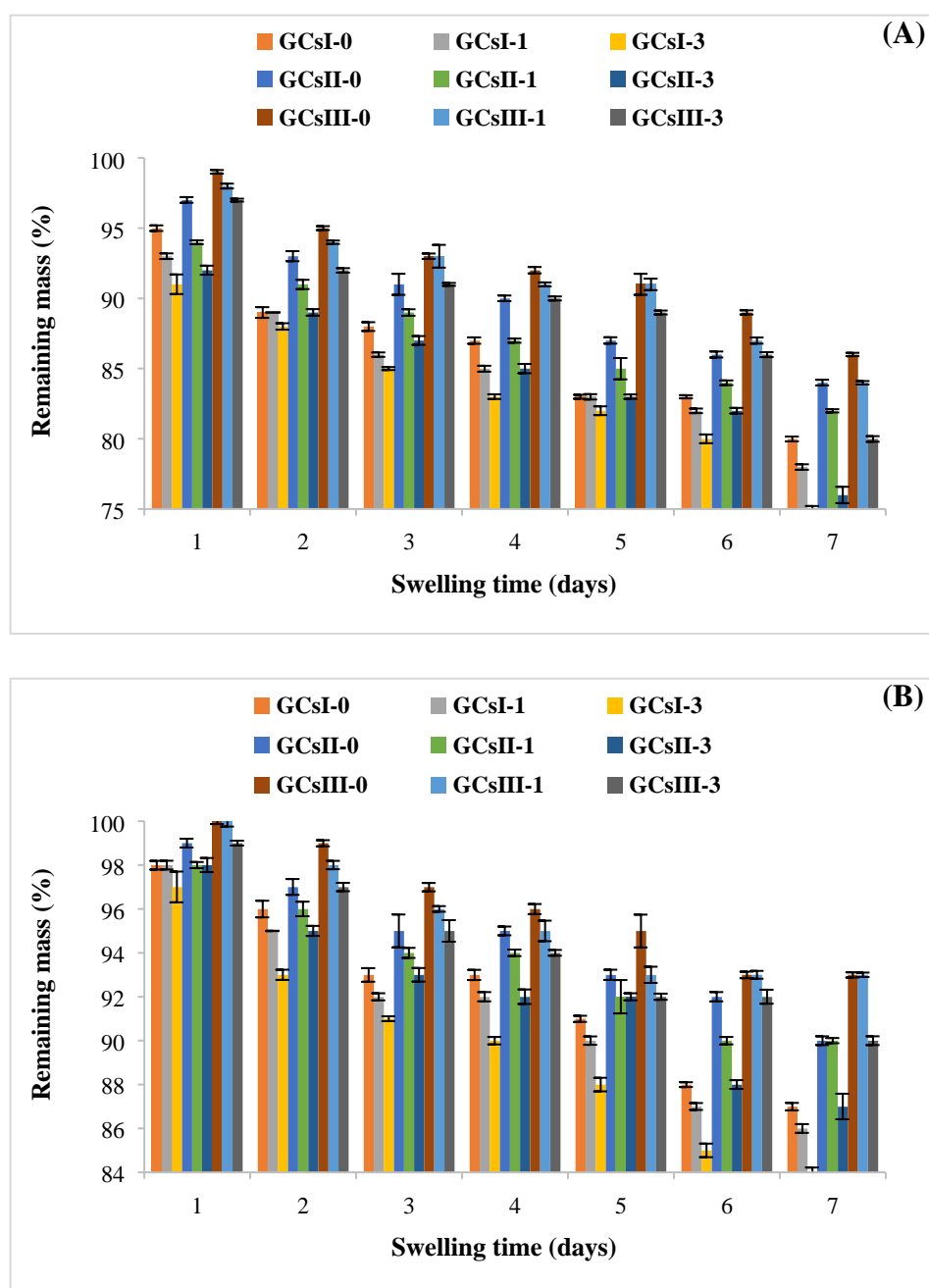


**Fig. 6**

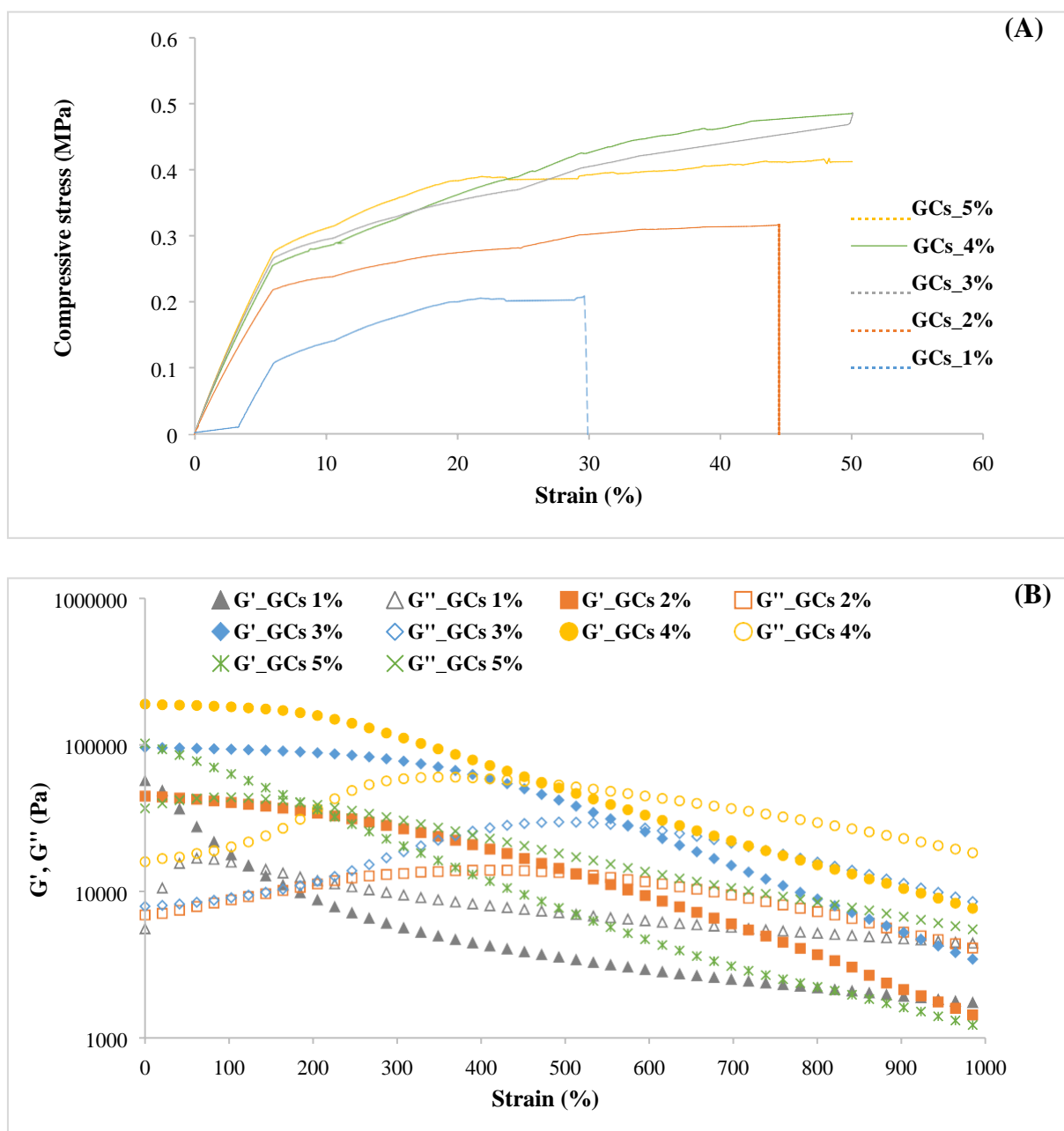




**Fig. 7**

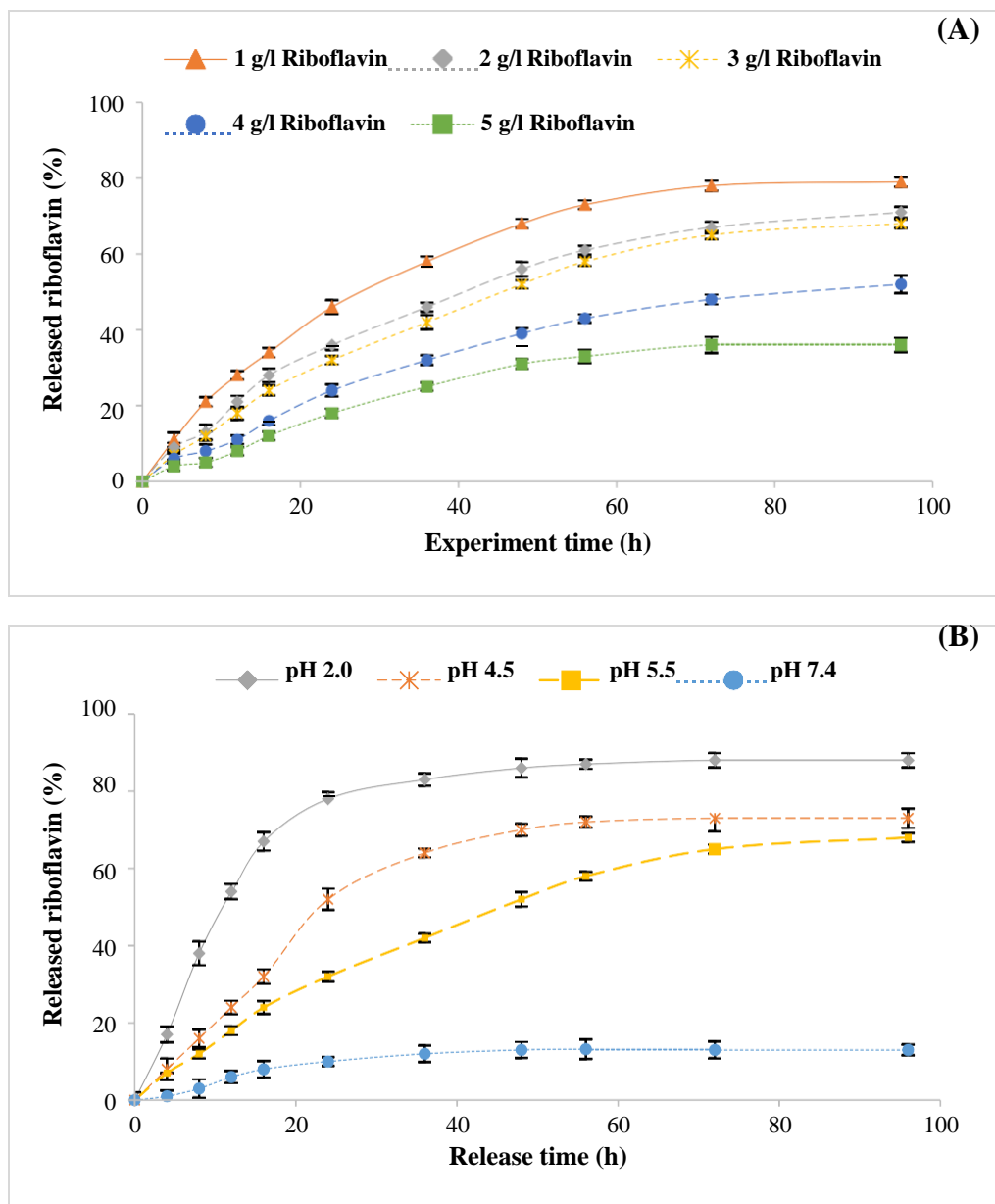


**Fig. S1**

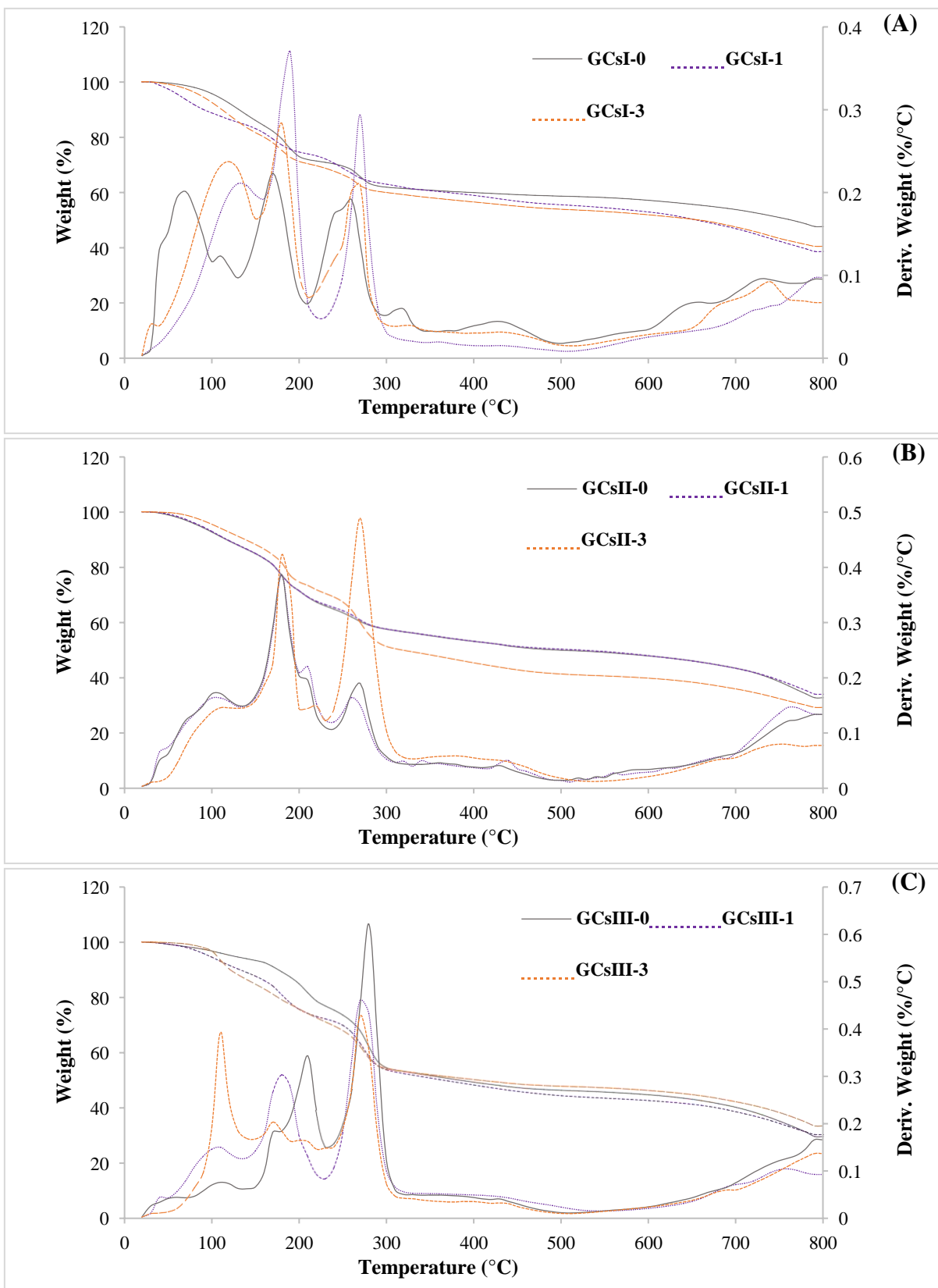
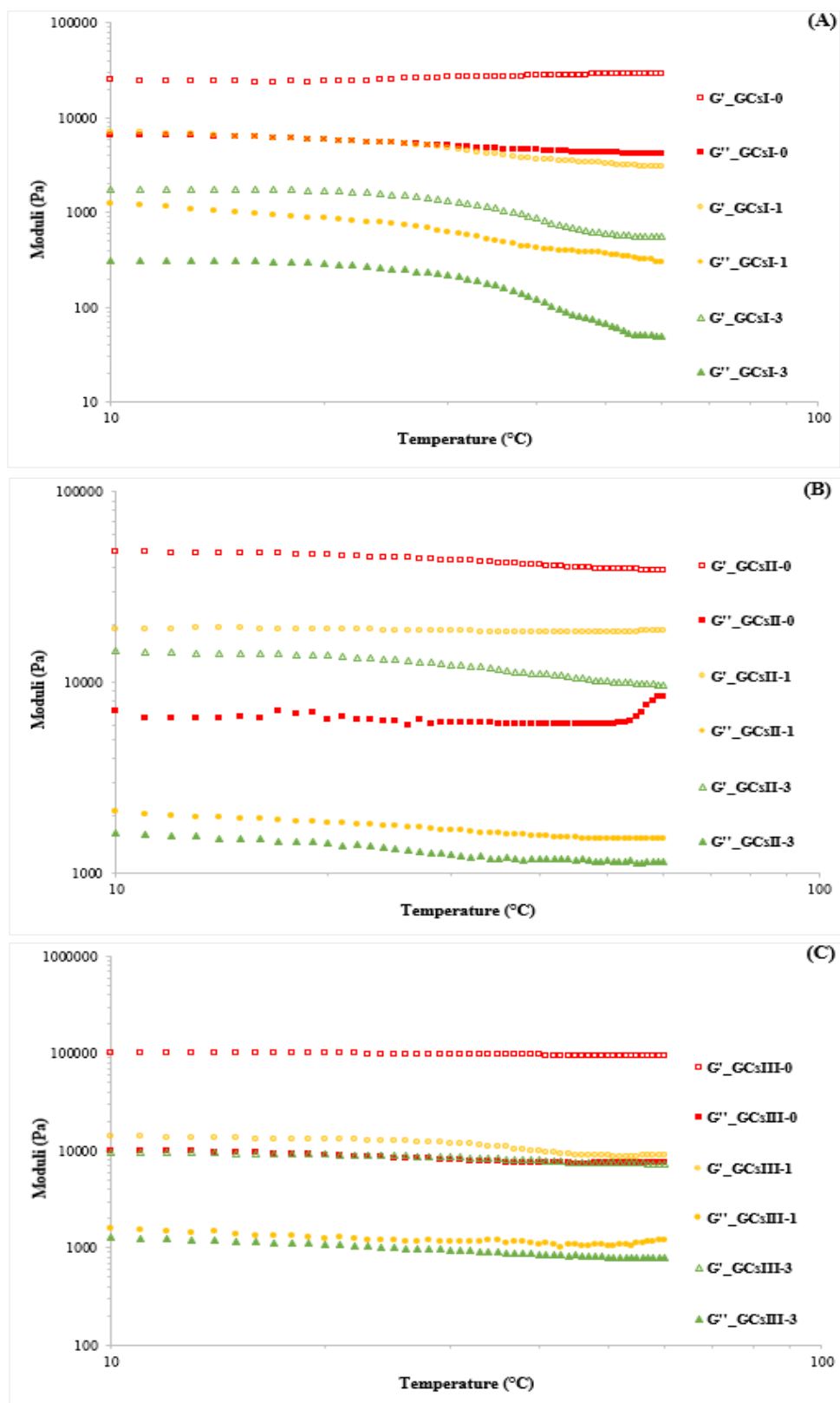


Fig. S2



**Table 1:** Moisture content (MC) and swelling ratio (SR) of different prepared Cs-based hydrogels.

Cs-based hydrogels	3% (w/v) Cs content					
	GCsI		GCsII		GCsIII	
	MC (%)	SR (g/g)	MC (%)	SR (g/g)	MC (%)	SR (g/g)
<b>GCs-0</b>	82.36±0.72 <sup>aB</sup>	13.59±0.45 <sup>aA</sup>	81.34±0.22 <sup>aB</sup>	16.57±1.04 <sup>aB</sup>	79.90±0.09 <sup>aA</sup>	18.10±0.47 <sup>aC</sup>
<b>GCs-1</b>	86.52±1.35 <sup>bC</sup>	14.92±0.32 <sup>bA</sup>	81.78±0.11 <sup>aB</sup>	18.93±0.32 <sup>bB</sup>	80.26±0.04 <sup>bA</sup>	22.21±0.53 <sup>bC</sup>
<b>GCs-3</b>	89.08±0.69 <sup>cC</sup>	16.38±0.27 <sup>cA</sup>	83.20±0.06 <sup>bB</sup>	22.86±0.78 <sup>cB</sup>	81.83±0.08 <sup>cA</sup>	26.24±0.93 <sup>cC</sup>

Different letters (a-c) in the same column are significantly different as determined by ANOVA test (p<0.05).

Different letters (A-C) in the same line indicated significant differences within hydrogels based on Cs with different AD (p<0.05).

**Table 2:** Cs-based hydrogels degradation temperatures (**Td**: onset temperature of degradation, **Tmax**: maximum degradation temperature and **Tf**: temperature of the end of degradation), the weight loss ( $\Delta w$ ) and the residue (**R**).

Parameters		GCsI			GCsII			GCsIII		
		GCsI-0	GCsI-1	GCsI-3	GCsII-0	GCsII-1	GCsII-3	GCsIII-0	GCsIII-1	GCsIII-3
Phase I	$\Delta W$ (%)	11.46	15.69	18.93	8.66	12.14	12.73	5.65	10.30	14.75
	Td (°C)	27.32	33.30	40.93	30.03	37.75	42.75	36.39	41.71	45.47
	Tmax (°C)	114.47	104.49	66.35	118.10	109.02	104.49	133.54	109.93	106.35
	Tf (°C)	147.16	133.54	129.00	153.51	134.45	129.91	158.96	135.35	130.81
Phase II	$\Delta W$ (%)	13.30	14.43	10.72	20.95	21.24	22.50	17.18	18.19	14.04
	Td (°C)	147.16	133.54	129.00	153.51	134.45	129.91	158.96	135.35	130.81
	Tmax (°C)	184.38	176.21	169.85	188.01	179.84	172.58	208.89	179.84	175.30
	Tf (°C)	227.05	210.71	207.08	235.22	229.77	226.13	235.22	231.59	227.05
Phase III	$\Delta W$ (%)	12.42	16.59	18.63	29.34	15.52	15.29	28.77	29.72	23.29
	Td (°C)	227.05	210.71	207.08	235.22	229.77	226.13	235.22	231.59	227.05
	Tmax (°C)	268.81	266.09	261.55	269.72	267.00	262.46	279.71	274.26	273.35
	Tf (°C)	511.22	507.58	502.14	537.54	508.49	502.14	547.53	510.31	509.40
R (%)		38.68	40.53	47.69	29.58	33.05	34.34	29.88	30.59	33.70

**Table 3:** Riboflavin entrapment efficiency (EE) and loading capacity (LC) of CsIII-0 based hydrogel, at a concentration of 3% (w/v).

Riboflavin concentration (g/l)	EE (%)	LC (%)
1	75.58 ± 0.61 <sup>c</sup>	23.51 ± 1.26 <sup>a</sup>
2	80.64 ± 1.59 <sup>d</sup>	31.14 ± 0.94 <sup>b</sup>
3	84.54 ± 1.35 <sup>e</sup>	36.57 ± 1.45 <sup>c</sup>
4	66.28 ± 0.52 <sup>b</sup>	37.19 ± 0.62 <sup>c</sup>
5	53.27 ± 1.72 <sup>a</sup>	37.81 ± 1.32 <sup>c</sup>

Different letters (a-e) in the same column are significantly different as determined by ANOVA test (p<0.05).

**Table S1:** Blue crab chitosan (Cs) nomenclature and respective acetylation degrees (AD) and average molecular weights ( $\text{g mol}^{-1}$ ).

average molecular weights ( $\text{g mol}^{-1}$ ).				
Cs	—	AD (%)		
		17	13	8
Cellulase digestion reaction-time (h)	0	CsI-0	CsII-0	CsIII-0
	1	CsI-1	CsII-1	CsIII-1
	3	CsI-3	CsII-3	CsIII-3
Cs	—	AD (%)		
		17	13	8
Digestion reaction-time (h)	0	125 600	118 900	115 000
	1	17 800	59 270	78 430
	3	10 440	18 540	16 040

**Table S2:** Different blue crab chitosan-based hydrogels (GCs) feed compositions and respective nomenclature.

Cs-based hydrogels	3% (w/v) Cs content		
	CsI	CsII	CsIII
Cs-0	GCsI-0	GCsII-0	GCsIII-0
Cs-1	GCsI-1	GCsII-1	GCsIII-1
Cs-3	GCsI-3	GCsII-3	GCsIII-3